QSOX2 deficiency-induced short stature, gastrointestinal dysmotility and immune dysfunction

Article

Published Version

It is advisable to refer to the publisher's version if you intend to cite from the work. See Guidance on citing.

Article

QSOX2 Deficiency-induced short stature, gastrointestinal dysmotility and immune dysfunction

Check for updates

Avinaash V. Maharaj [1] ✉, Miho Ishida[1], Anna Rybak[2], Reem Elfeky[3], Afiya Andrews [1], Aakash Joshi[4], Frances Elmslie[5], Anni Joensuu [6], Katri Kantojärvi[6], Raina Y. Jia[7], John R. B. Perry [7], Edel A. O'Toole [8], Liam J. McGuffin [9], Vivian Hwa [10,11] ✉ & Helen L. Storr [1] ✉

Postnatal growth failure is often attributed to dysregulated somatotropin action, however marked genetic and phenotypic heterogeneity exist. We report five patients from three families who present with short stature, immune dysfunction, atopic eczema and gastrointestinal pathology associated with recessive variants in *QSOX2*. *QSOX2* encodes a nuclear membrane protein linked to disulphide isomerase and oxidoreductase activity. Loss of QSOX2 disrupts Growth hormone-mediated STAT5B nuclear translocation despite enhanced Growth hormone-induced STAT5B phosphorylation. Moreover, patient-derived dermal fibroblasts demonstrate Growth hormone-induced mitochondriopathy and reduced mitochondrial membrane potential. Located at the nuclear membrane, QSOX2 acts as a gatekeeper for regulating stabilisation and import of phosphorylated-STAT5B. Altogether, QSOX2 deficiency modulates human growth by impairing Growth hormone-STAT5B downstream activities and mitochondrial dynamics, which contribute to multisystem dysfunction. Furthermore, our work suggests that therapeutic recombinant insulin-like growth factor-1 may circumvent the Growth hormone-STAT5B dysregulation induced by pathological *QSOX2* variants and potentially alleviate organ specific disease.

Short stature, a potential indicator of underlying maladies, is defined as height for age more than 2 deviations below the population median (~ 2% of the population) and is the commonest reason for referral to paediatric endocrinology clinics[1]. Although adult height is 80–90% heritable[2], the molecular basis for growth failure in 50–90% of patients remains unidentified despite advances in genomic sequencing strategies[1].

Defects in growth hormone (GH) action account for a substantial percentage of endocrine causes of growth failure but are frequently unrecognised due to wide clinical and biochemical variability. Marked

[1]Centre for Endocrinology, John Vane Science Centre, Queen Mary University of London, Charterhouse Square, London, UK. [2]Gastroenterology Department, Great Ormond Street Hospital, London, UK. [3]Immunology Department, Great Ormond Street Hospital, London, UK. [4]St George's University Hospitals NHS Foundation Trust, London, UK. [5]Genomics Clinical Academic Group, St George's University Hospitals NHS Foundation Trust, London, UK. [6]THL Biobank, the Department of Knowledge Brokers, Finnish Institute for Health and Welfare, Helsinki, Finland. [7]MRC Epidemiology Unit, University of Cambridge, School of Clinical Medicine, Cambridge, UK. [8]Centre for Cell Biology and Cutaneous Research, Blizard Institute, Queen Mary University of London, London, UK. [9]School of Biological Sciences, University of Reading, Reading, UK. [10]Cincinnati Children's Hospital Medical Center, Department of Pediatrics, University of Cincinnati College of Medicine, Cincinnati, Ohio, USA. [11]Premium Research Institute for Human Metaverse Medicine (WPI-PRIMe), Osaka University, Suita, Osaka, Japan. ✉e-mail: a.v.maharaj@qmul.ac.uk; hwa.vivian.prime@osaka-u.ac.jp; h.l.storr@qmul.ac.uk

genetic and phenotypic heterogeneity exist, with heritable defects in genes downstream of the GH receptor (GHR) or interacting pathways accounting for a significant number of non-classical cases[3]. Homozygous inactivating variants in signal transducer and activator of transcription (*STAT5B*), a key effector of GH-GHR regulated production of the growth-promoting insulin-like growth factor 1 (IGF-1), cause classical GH insensitivity (GHI) with severe postnatal growth failure and IGF-1 deficiency. *STAT5B* loss of function of variants leads to immune dysregulation, which exists on a continuum with features ranging from eczema, opportunistic infections, progressive immunodeficiency, autoimmunity and pulmonary compromise[4–9]. Milder phenotypes, with variable degrees of GHI and immunodeficiency, have been characterised in dominant negative *STAT5B* heterozygotes[4]. We now report probands with milder phenotypes akin to dominant negative *STAT5B* heterozygotes but associated with a regulatory interactor of STAT5B which, when absent, blunts STAT5B-mediated regulation of IGF-1 expression by impairing STAT5B nuclear translocation.

QSOX2 (Quiescin sulfhydryl oxidase 2, MIM 612860), a multidomain enzyme, belongs to a family of sulfhydryl oxidases best known for catalysing the introduction of disulphide bonds in secreted proteins. *QSOX2* shares a 41.2% sequence homology with *QSOX1*, a well-characterised sulfhydryl oxidase shown in vitro to be protective against oxidative stress-mediated cell death[10–12]. Contrastingly, the poorly characterised QSOX2, a ubiquitously expressed protein, localises to the nuclear membrane/nucleoplasm and Golgi apparatus. No pathological defects in either *QSOX1* or *QSOX2* have been reported, although two genome-wide association studies have identified *QSOX2* polymorphisms in association with height[13,14]. A study of 19,633 Japanese subjects, identified the *LHX3-QSOX2* locus as a significant adult height quantitative trait locus (QTL)[13]. More recently, meta-analyses of large genetic data repositories identified 12,111 height-associated SNPs, of which two *QSOX2* polymorphisms (rs7024579 and rs7038554) were significantly associated with height in European populations[14]. However, to date, clinically relevant *QSOX2* variants associated with postnatal growth failure or other phenotypes, have not been reported.

We describe the first pathological *QSOX2* variants discovered by next-generation sequencing of five individuals with short stature. We demonstrate a direct interaction between QSOX2 and STAT5B. All variants lead to robust GH-stimulated tyrosine phosphorylation of STAT5B. STAT5B nuclear translocation was attenuated with resultant reduced STAT5B downstream transcriptional activities. Intriguingly, robust GH-induced STAT5B phosphorylation correlated with the reorganisation of oxidative phosphorylation complexes and diminished mitochondrial membrane potential in patient-derived dermal fibroblasts. Collectively, QSOX2 deficiency abrogates downstream STAT5B activity, causing a unique syndrome with additional features of atopic eczema, feeding difficulties, gastrointestinal dysmotility and recurrent infections.

Results
Clinical phenotypes of Index Family 1 probands
Identical male twins, probands P1 (Twin 1) and P2 (Twin 2), from a non-consanguineous British European/South Asian kindred (Fig. 1A), were born at 30 weeks gestation with a birth weight appropriate for gestational age. They presented at age 1.3 years with significant postnatal growth failure (UK-WHO growth reference height and weight standard deviation scores (SDS) of − 3.9 and − 2.6 and − 5.0 and − 3.3, respectively) (Fig. 1B and Table 1). Bone age was concordant with chronological age. Feeding difficulties associated with reduced gastrointestinal motility and oral aversion, chronic refractory constipation, oesophageal reflux, and recurrent episodes of gastroenteritis were more pronounced in P2, whose oral feeding aversion necessitated insertion of a percutaneous endoscopic gastrostomy (PEG) feeding tube at age 2.8 years. Hindgut dysmotility was confirmed

with rectal outlet dysfunction in P1 and a mixed-type of slow colonic transit with rectal outlet dysfunction in P2 (Fig. 1C, D), requiring laxative and stimulant treatment as well as repeated injections of botulinum toxin into the anal sphincter. Weight and BMI standard deviation scores remained low but stable with optimised nutritional status as evidenced by normal vitamin and trace element levels, but linear growth remained significantly impaired. Skeletal surveys and developmental milestones were normal.

GH-provocation testing elicited a normal GH response for P2, the disparate peak GH response in P1 may be explained by significant technical difficulties (see Table 1 legend). Basal IGF-1 levels remained consistently low in both probands, with serum IGFBP-3 within normal ranges, consistent with partial GH insensitivity (GHI)[15,16]. Collectively, the clinical picture was suggestive of primary post-natal growth failure. Both probands exhibited mild dysmorphism with prominent forehead and downward slanting palpebral fissures and mild immune dysregulation characterised by atopic eczema, asthma, recurrent respiratory tract infections and cows' milk protein, soy, and egg allergies. These additional clinical features, in association with postnatal growth failure and persistently low IGF-1 levels, overlapped with those of STAT5B deficiency (MIM 245590), a growth disorder associated with variable degrees of immunodeficiency[7,17]. Peripheral blood immune profiling revealed persistently low IgM levels, raised gamma delta and double negative T cells denoting immune dysregulation. Basal levels of tyrosine phosphorylated STAT5 (p-STAT5) in peripheral blood mononuclear cells (PBMC) were elevated compared to controls (1.9% in control vs. >7% in probands). Interferon (IFN) signature gene assay revealed equivocal Type I IFN-inducible gene expression, but both twins demonstrated significant downregulation of SIGLEC1 (sialic acid binding Ig like lectin 1; Table 2). CT chest with contrast showed no evidence of lung fibrosis, a well-reported feature in patients with homozygous STAT5B deficiency.

Initial genetic testing, including karyotyping and PTEN sequencing, did not reveal a unifying diagnosis. Furthermore, microarray-based comparative genomic hybridisation yielded no significant copy number variations. Targeted genome sequencing revealed no pathogenic variants in *STAT5B* or other common growth-related genes, including the key genes of the GH-IGF-1 axis, whilst methylation analyses of both imprinted domains associated with short stature at 11p15.5, H19DMR and KvDMR (MS-MLPA) were normal. We undertook whole exome sequencing (WES), which corroborated the targeted gene panel sequencing data. Intriguingly, the top candidate variants were compound heterozygous variants in *QSOX2*, a gene in which no pathological variants have been reported to date. These were a novel paternally-inherited single base deletion (*c.973delG*) predicted to result in a frameshift and truncated protein (p.V325Wfs*26) and a maternally-inherited missense variant rs61744120, (*c.1055 C > T*, p.T352M) with a MAF of 0.008509 (gnomAD), predicted deleterious by several computational platforms (SIFT, PolyPhen-2 and CADD). Despite the subtle predicted conformational change to the QSOX2 protein, thermostability analysis deemed the p.T352M variant to be destabilising (Supplementary Fig. 1A, B). Both variants are located in exon 8 of the *QSOX2* gene and precede the ERV/ALR sulfhydryl oxidase domain, which is lost in the frameshift truncation and likely impacted by the thermally unstable p.T352M substitution (Fig. 2A).

As recombinant human GH treatment can improve growth in partial GHI[3,18], a trial of rhGH therapy was initiated at 4.5 years (dose 0.025 mg/kg/day; 0.3 mg/day). Following 1.5 years of therapy, modest increases in height and weight SDS (+ 0.7 and + 0.4 in P1, and + 0.9 and + 0.6 in P2, respectively) were observed with normalisation of serum IGF-1.

Clinical phenotypes of Index Family 2 probands
Proband P3, a female from a consanguineous Pakistani kindred (Fig. 1A) was enrolled in the U.K. 100,000 Genomes Project during
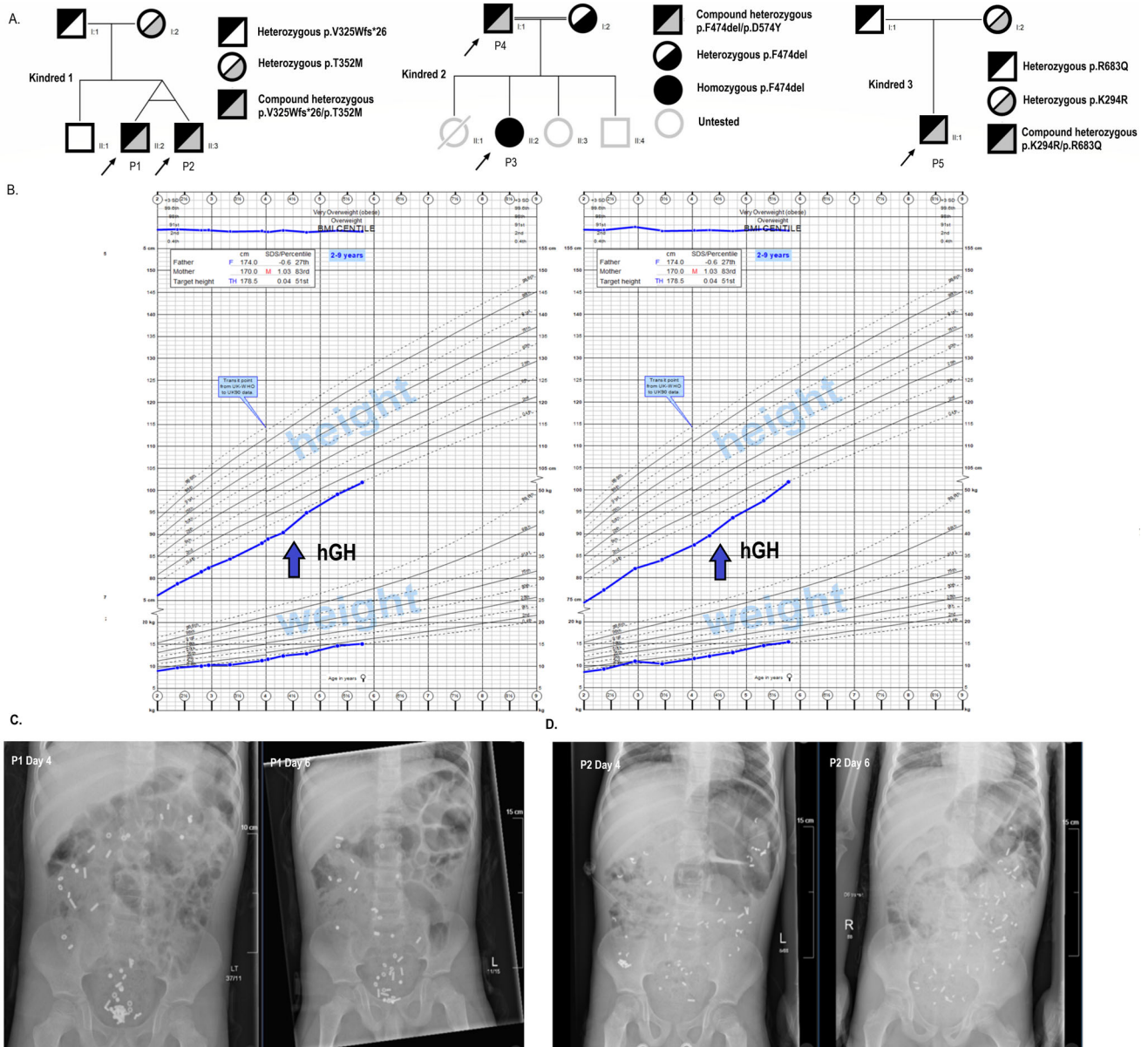
Fig. 1 | Pedigree charts of all families and anthropometric analyses of Kindred 1.
A Inheritance of *QSOX2* variants delineated across two generations for each
respective kindred. **B** Height, weight, and BMI centile growth charts (2–9 yrs) of
probands 1 and 2, generated by Growth XP (PC PAL version 2.8). GH indicates when
recombinant growth hormone therapy (0.025 mg/kg/day) was commenced. Most
recent measurements suggest a modest improvement in height trajectories.
C Colonic marker transit studies for probands 1 and 2 were performed after bowel

dis-impaction. Patients ingested 10 differently shaped markers for three con-
secutive days. Plain abdominal X-rays were performed on days 4 and 6 post-first
marker ingestion. Colonic marker transit study of proband 1 was indicative of rectal
outlet dysfunction. **D** Abdominal X-rays for colonic marker transit study in proband
2 indicate a mixed type of rectal outlet dysfunction and slow colonic transit
(retention of innumerable markers).

adolescence with intractable eczema and lichen planus associated
with elevated IgE levels. She was born appropriate for gestational
age and demonstrated early postnatal growth retardation asso-
ciated with feeding difficulties. Despite exhibiting moderate catch-
up growth, the patient presented at the age of 3 years with
intractable asthma, extensive eczema, allergy rhinitis, recurrent
respiratory tract, bacterial skin infections and gastrointestinal
dysmotility (Table 1).

P3 was identified by interrogating the 100,000 Genomes Pro-
ject rare disease cohort for subjects harbouring potentially causa-
tive *QSOX2* variants, utilising HPO terms related to short stature,
eczema and immune dysfunction. P3, with relevant phenotypic
features, harboured a recessive homozygous *QSOX2* variant. The
variant, an in-frame p.F474del deletion with a MAF of 0.00001314

(gnomAD; no homozygotes), was predicted disease-causing by
Mutation Taster[19].

At age 24 years, P3 had an adult height SDS of − 1.9 and continued
to experience recurrent severe eczema and constipation. Genotyping
of family members revealed both parents were heterozygous for the
p.F474del variant. The patient's mother was asymptomatic with nor-
mal height (− 0.4 SDS). The patient's father (proband 4; P4) had short
stature (height − 2.2 SDS) and harboured an additional de novo mis-
sense variant in *QSOX2* (*c.1720 G > T*, p.D574Y), absent in other family
members tested. This variant was predicted deleterious by SIFT and
PolyPhen-2. P3's two younger siblings, an asymptomatic sister aged 15
(height -0.4 SDS) and a brother aged 18 years with short stature (height
− 2.0 SDS), constipation and chronic bowel inflammation, declined to
participate in this study.

Table 1 | The clinical and biochemical profiles of the probands harbouring bi-allelic *QSOX2* variants

	Proband 1 (P1, Twin 1)	Proband 2 (P2, Twin 2)	Proband 3 (P3)	Proband (P4)	Proband 5 (P5)
Sex	Male	Male	Female	Male	Male
Gestational age (weeks)[a]	30	30	40	–	39
Birth weight (kg)	1.3	1.0	3.2	–	3.5
Birth weight SDS	−0.5	−1.6	−0.5	–	+0.6
	Auxology (aged 1.3 yrs)		Auxology (aged 24 yrs)	Auxology (aged 53 yrs)	Auxology (aged 4.8 yrs)
Height (cm)	69.8	67.0	152.7	163.4	97.2
Height SDS[b]	−3.9	−5.0	−1.9	−2.2	−2.5
Weight (kg)	7.9	7.2	47.6	69.2	15.2
Weight SDS[b]	−2.6	−3.3	−1.5	−1.27	−1.2
BMI SDS	−0.2	−0.3	−0.77	0.92	0.6
Target height SDS	0.04	0.04	–	–	1.0
HC SDS	0.1	−0.1	–	–	0.73
Clinical features					
Downslanted palpebral fissures	Yes	Yes	No	No	No
Allergies	Egg, soy, milk	Egg, soy, milk	No	No	No
Recurrent Respiratory infections	Yes (prophylactic azithromycin)	Yes (prophylactic azithromycin)	Yes (in childhood)	No	Yes (in infancy)
Asthma	Yes	Yes	Yes	No	No
Atopic eczema	Yes	Yes	Yes	No	Yes
Gastrointestinal disturbance	Chronic constipation, recurrent gastroenteritis, gastro-oesophageal reflux	Oral feeding aversion requiring PEG, chronic constipation, recurrent gastroenteritis, gastro-oesophageal reflux	Constipation	Bile acid malabsorption, cholelithiasis	Poor feeding, Gastro-oesophageal reflux
Other	Recurrent fractures on minor trauma	Hypospadias, bilateral inguinal hernias	–	–	Motor developmental delay, Hyper-pigmented macules
Radiological					
Bone age (yr)	1.3	1.3	–	–	–
Pituitary MRI	Normal	Normal	–	–	–
Skeletal survey	Normal	Normal	–	–	–
Chest CT with contrast	Normal	Normal	–	–	–

[a]Placental insufficiency from 16 weeks gestation and born by emergency caesarean section. GH provocative testing was undertaken using glucagon stimulus with GH < 6.7 µg/L indicative of GH deficiency (UK guidance). There were several issues with GH-provocation testing in proband 1 (Glucagon), mostly due to multiple attempts at cannulation prior to stimulation. The patient (P1) became hypoglycaemic early on, with a nadir blood glucose of < 3.3 mmol/L, necessitating abandoning testing before a 'potential peak GH level' was attained. Typical for young children with severe GHD or GH insensitivity, there was a history of recurrent spontaneous hypoglycaemia in probands 1 and 2. This may have led to a degree of desensitisation and an inability to mount a prodigious GH response to hypoglycaemia[67]. Furthermore, the test was only performed once (given the age and distress incurred to the patient), and multiple sources of evidence show poor sensitivity/specificity of single provocation studies and variable responses depending on the stimulus used[67,68].

[b]Height, weight and target height standard deviation scores (SDS) were calculated using the sex and age-appropriate UK-WHO references (PCPAL GrowthXP version 2.8). Hypospadias and inguinal hernia repairs in P2 (Twin 2) aged 2.5 yr. Bone age calculated by BoneXpert 3.0 (Visiana) at a chronological age of 1.3 years. NR, normal range; HV, height velocity; HC, head circumference.

Clinical phenotype of Index Family 3 proband

Proband P5, a British European male (Fig. 1A), was enrolled in the U.K. 100,000 Genomes Project at 4.8 years with postnatal growth restriction, failure to thrive and motor developmental delay. He was born appropriate for gestational age and demonstrated early postnatal growth retardation associated with poor feeding and frequent infections in the neonatal period. The patient presented at the age of 2.5 years with delayed fine and gross motor development, dystonic posturing, eczema, hyper-pigmented skin macules, short stature and gastro-oesophageal reflux (Table 1). Biochemically, the proband demonstrated features of primary IGF-1 deficiency (growth hormone insensitivity) with an IGF-1 SDS of −2.0 associated with an adequate GH peak of 11 µg/L on provocation testing. Interferon (IFN) gene profiling revealed no evidence of interferonopathy, but IFI27 levels were elevated. (Table 2).

Interrogation of the 100,000 Genomes Project rare disease cohort revealed that P5 harboured bi-allelic compound heterozygous variants in *QSOX2*; A paternally inherited missense variant, (*c.2048*

G > A, p.R683Q) with a MAF of 0.000003989 (gnomAD; no homozygotes) and predicted deleterious by several computational platforms (SIFT, PolyPhen-2 and CADD) and; a maternally inherited single amino acid substitution, (*c.881 A > G*, p.K294R) with a MAF of 0.00001971 (gnomAD; no homozygotes), predicted damaging by CADD and Mutation taster but tolerated by SIFT and PolyPhen-2.

Protein-altering variants significantly correlate with height

In 420,162 individuals of European ancestry in the UK Biobank (UKBB), we identified 200 carriers of 39 rare (MAF < 0.1%) protein truncating variants (PTVs) in *QSOX2*. In combination, these PTVs were associated with reduced adult height (beta: −1.13 cm, 95% CI: −0.45- to −1.8, $p = 0.001$).

A role for *QSOX2* in the regulation of adult height was also supported by a reported genome-wide significant common variant signal within its first intron (rs7038554-G, beta = 0.023 standard deviations, 95% CI = 0.021-0.024, $p = 8.82 \times 10^{-154}$, $n = 3,922,710$)[14]. The height-increasing allele also confers increased *QSOX2* mRNA levels in

Table 2 | Immunological testing and interferon signature gene profiles of probands

	Proband 1 (P1, Twin 1)	Proband 2 (P2, Twin 2)	Proband 3 (P3)	Proband 4 (P4)	Proband 5 (P5)
Immunology					
IgA, IgG	Normal	Normal			Normal
IgM (g/L) (NR 0.5-2.2)	0.2	0.3			0.6
IgE (IU/ml) (NR < 52)	Normal	Normal			Normal
T and B cells[a]	Normal	Normal			Normal
Naïve CD4 and naïve CD8	Normal	Normal			Normal
Class switched memory B cells	Normal	Normal			Normal
Transitional B cells	Normal	Normal			Normal
CD21 low B cells	Normal	Normal			Normal
CD4 + CD25+FoxP3+	Normal	Normal			–
Gamma delta T cells (NR 1-5%)	12.2%	12.9%			–
Double negative T cells (NR < 2%)	4.4%	2.7%			–
Vaccine responses to tetanus and pneumococcal protein vaccine	Normal	Normal			–
Complement levels; C3 and C4	Normal	Normal			Normal
STAT5 ptyr (%) (control 1.9%)	7.7	7.7			–
Interferon signature gene assay					
CXCL10 (NR 0.28-5.31)	0.69	0.45			0.57
CXCL9 (NR 0.28-2.39)	0.82	0.36			0.75
IFI27 (NR 0.09-2.24)	0.18	2.23			3.58
IFI44L (NR 0.24-7.18)	0.28	0.34			1.76
IFIT1 (NR 0.17-5.84)	0.27	0.31			2.36
IFNB1 (NR 0.23-14.12)	0.31	0.21			0.43
IFNG (NR 0.33-2.59)	0.49	0.91			0.33
IL-18 (NR 0.67-1.30)	0.68	0.66			1.25
ISG15 RSAD2 (NR 0.19-6.86)	0.19	0.20			1.21
SIGLEC1 (NR 0.17-4.66)	0.05	0.03			0.28

[a]Immunology tests confirmed normal T cell number with normal proliferation to the mitogen PHA, and B cells were normal with normal tetanus and pneumococcus vaccine responses. STAT5 ptyr (STAT5 tyrosine phosphorylation) at baseline was increased, and there were normal responses to IL-2, 7 and 15.

several tissues[20], an effect directionally consistent with the above impact of rare PTVs.

Interestingly, we also identified 6371 adults in UKBB (MAF 0.7%) who harboured the *c.1055 C > T* variant (p.T352M, rs61744120). Of these, 31 were homozygotes whose adult heights ranged from − 1.7 SDS to + 2.0 SDS (mean − 0.28, SD 1.02; Supplementary Table 1). Across all carriers of *c.1055 C > T*, an additive model showed a non-significant association with adult height ($p = 0.49$).

SNP rs61744120 is enriched in the Finnish population

The *QSOX2 c.1055 C > T*, p.T352M variant (rs61744120) has a MAF of 0.05197 in the Finnish population[21]. Cross-validation of FinnGen SNP array data with whole genome sequence data in FINRISK identified 16 homozygotes of *c.1055 C > T*, of whom 15 had adult height SDS values below the population average (range − 0.1 to − 2.5 SDS; Supplementary Tables 2 and 3). In contrast to UKBB, across all carriers of *c.1055 C > T* in FINRISK, an additive model showed an association with shorter adult height ($p = 0.0154$, adjusted for age and sex).

### SNP rs61744120 may be associated with aberrant splicing

Given the height variability demonstrated among homozygotes for this variant, we postulated that alternative splicing transcripts might occur in vivo despite predictions from in silico computational platforms, human splicing finder[22] and MaxEntScan[23], which suggested no impact on splicing. In vitro splicing assays (Supplementary Fig. 1C) revealed the presence of two transcripts (Supplementary Fig. 1D) for the homozygous p.T352M variant, one consistent with unaltered splicing (489 bp) and a smaller transcript demonstrating exon 8 skipping (359 bp) (Supplementary Fig. 1E). This aberrantly spliced transcript,

which likely occurs due to naturally weak canonical splice sites, is predicted to result in a frameshift p.N319Kfs*51, possibly undergoing degradation by nonsense-mediated mRNA decay. Notably, in patient (P2) fibroblasts which harbour this variant in heterozygosity, RT-PCR using coding primers spanning exons 7–9 of *QSOX2* revealed the presence of two transcripts, one consistent with wild type product (320 bp) and a minor, smaller transcript, (190 bp) consistent with the skipping of exon 8 (130 bp) (Supplementary Fig. 1E). These observations support low occurrence of abnormal splicing events due to SNP rs61744120 (*QSOX2 c.1055 C > T* variant).

p.T352M and p.V325Wfs*26 cause robust p-STAT5B responses

In GH-mediated post-natal growth, the binding of GH to hepatic GHR leads to STAT5B recruitment to activated GHR, whereupon STAT5B is tyrosine phosphorylated, homodimerized and translocated to the nucleus to function as a transcription factor regulating the expression of target genes including *IGF1* and *IGFBP3*. Dysregulation of this pathway can cause partial or atypical GHI, which, in part, explains the varying therapeutic efficacy of rhGH or rhIGF-1 treatments. Since the in vivo phenotype of our patients was suggestive of partial GHI, the role of QSOX2 in GH-mediated growth was investigated.

Since the *QSOX2 c.1055 C > T* variant resulted in predominant expression of the missense variant, p.T352M, we assessed the expression and function of p.T352M in our established in vitro HEK293-hGHR reconstitution system. Expression of QSOX2 p.T352M was markedly reduced when compared to wild-type (WT) QSOX2 (Fig. 2A), corroborating in-silico thermostability predictions. A protein of lower mass was visualised for p.V325Wfs*26 consistent with a frameshift truncation (Fig. 2B). Immuno-fluorescent analyses of FLAG-tagged
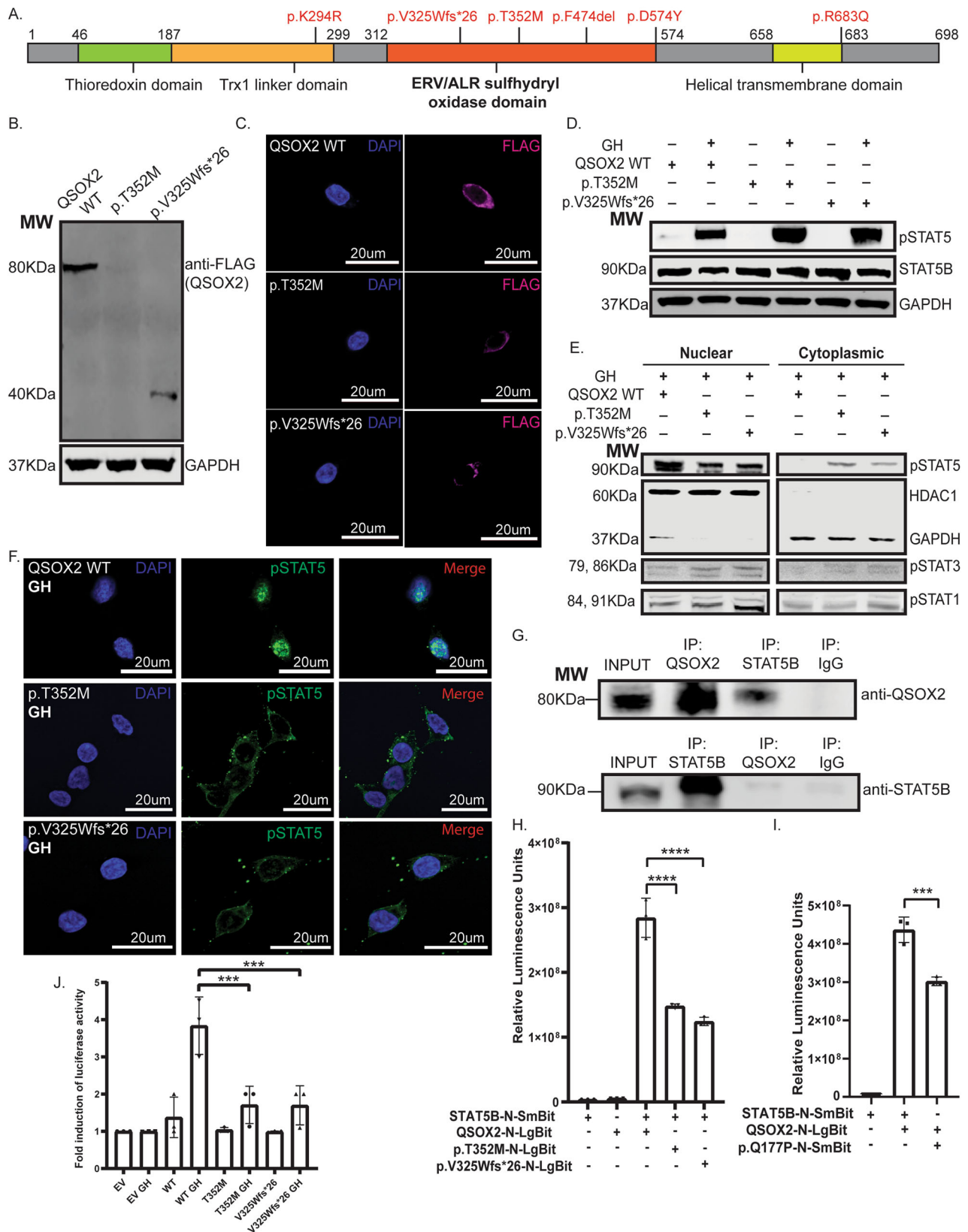
constructs, revealed a diminished abundance of both variants at the nuclear membrane when compared to WT-QSOX2 (Fig. 2C).

We next treated *QSOX2* variant-transfected cells with recombinant GH and assessed STAT5B signalling. Intriguingly, although tyrosine phosphorylation of STAT5B (p-STAT5) was more robust in the presence of the QSOX2 variants than WT-QSOX2 (Fig. 2D), p-STAT5

was not associated with increased nuclear shuttling, confirmed by subcellular fractionation analysis (Fig. 2E). Nuclear p-STAT5 levels were markedly and reproducibly reduced in the presence of both variants compared to WT-QSOX2, with p-STAT5 cytoplasmic accumulation observed by immunofluorescent microscopy (Fig. 2F). Notably, the impact of QSOX2 deficiency was restricted to STAT5 since GH-induced

Fig. 2 | Loss of function variants in *QSOX2* negatively impact STAT5B functions.
A Schematic of QSOX2 protein with key domains, including the relative location of
QSOX2 variants identified in probands P1-P4. **B** Immunoblotting of FLAG-tagged
QSOX2 cDNA constructs showed that expression of both variants was reduced
compared to wild-type (WT)-QSOX2, with expected truncated protein due to early
protein termination observed for p.V325Wfs*26. **C** Immunofluorescent microscopy
demonstrated a reduction in QSOX2 peri-nuclear expression for both variants when
compared to WT-QSOX2. **D** Immunoblot analyses of transfected HEK 293-hGHR
cell lysates demonstrated that p-STAT5 was markedly enhanced in the presence of
both variants following GH stimulation. **E** Nuclear and cytoplasmic fractions of
transfected HEK 293-hGHR cells demonstrated a reduction of p-STAT5 in nuclear
fractions of both variants with concomitant cytoplasmic abundance of p-STAT5
when compared to wild type. Nuclear levels of p-STAT3 and p-STAT1 were indis-
tinguishable between both variants and the wild type. **F** Immunofluorescent
microscopic analysis of GH-stimulated transfected HEK 293-hGHR cells showed
nuclear translocation impairment of p-STAT5 for both QSOX2 variants but not with
WT-QSOX2. **G** Co-immunoprecipitation and immunoblot analysis of WT-QSOX2-
STAT5B interactions showed a direct protein-protein interaction between

unstimulated WT-QSOX2 and STAT5B. **H** NanoBit complementation assays showed
that the robust interaction seen between QSOX2-WT and STAT5B-WT was atte-
nuated for both p.T352M ($p < 0.0001$) and p.V325Wfs*26 ($p < 0.0001$). Ordinary
one-way-ANOVA was used for statistical analysis with multiple testing corrections
performed using Sidak's test. **I** NanoBit complementation assays showed a sig-
nificant reduction in interaction affinity for the pathogenic variant p.Q177P known
to abrogate nuclear STAT5B import ($p = 0.0004$), supporting the importance of
QSOX2 for STAT5B nuclear localisation. Ordinary one-way-ANOVA was used for
statistical analysis with multiple testing corrections performed using Dunnett's test.
J In vitro STAT5B transcriptional activities were evaluated by dual luciferase growth
hormone response element (GHRE) reporter assay. The 4-fold increase in GH-
induced luciferase activities in the presence of WT-QSOX2 (WT), was significantly
blunted in the presence of QSOX2 variants ("T352M", $p = 0.0001$; "V325Wfs*26",
$p = 0.0001$). Ordinary one-way-ANOVA was used for statistical analysis with multi-
ple testing corrections performed using Sidak's test. Source data are provided as a
Source Data file. Data are presented as the mean ± SD of three repeated measure-
ments (3 independent replicates).

phosphorylation and nuclear localisation of STAT3 and STAT1 in the
presence of both variants were analogous to WT-QSOX2 (Fig. 2E).
Dimerisation of p-STAT5, utilising our generated *QSOX2* deficient iso-
genic cell line (Supplementary Fig. 2A, B), was unimpeded. We con-
clude that nuclear import of GH-stimulated p-STAT5 requires
functional QSOX2.

QSOX2 directly interacts with STAT5B
We next investigated possible interactions between QSOX2 and
endogenous STAT5B. From HEK 293-hGHR cell lysates overexpressing
WT QSOX2, unstimulated endogenous STAT5B and QSOX2 were
readily co-immunoprecipitated (co-IP) (Fig. 2G). To negate potential
co-IP interferences by antibodies, we also evaluated protein-protein
interaction by Nanoluc Binary technology (NanoBit). Reporter-tagged
target proteins were generated, and, through complementation
assays, positive WT reporter fragment interaction was detected as
robust luminescent activity. Importantly, this interaction was dis-
rupted when QSOX2 variants were assayed against WT-STAT5B
(Fig. 2H). The critical role of QSOX2 in binding and facilitating
STAT5B nuclear localisation was supported by demonstrating a
markedly reduced interaction of WT-QSOX2 with a well-expressed
dominant-negative STAT5B p.Q177P variant known to be unable to
translocate to the nucleus[4] (Fig. 2I).

The consequence of impaired STAT5B nuclear translocation is
impaired transcriptional activities as assessed by GHRE dual luciferase
reporter assays, with induction of luciferase activity significantly
reduced in the presence of both QSOX2 variants (Fig. 2J). Collectively,
disruption of QSOX2-STAT5B interactions, either through QSOX2
deficiency or STAT5B defects, significantly impairs STAT5B nuclear
localisation and transcriptional activities.

In frame deletion p.F474del similarly disrupts STAT5B nuclear localisation
Expression of QSOX2 p.F474del (identified in P3) was markedly
reduced when compared to wild-type (WT) QSOX2 both on immuno-
blotting and immunofluorescence (Fig. 3A, B). GH stimulation elicited
robust p-STAT5 in the presence of the p.F474del variant (Fig. 3C),
although nuclear fractions demonstrated reduced levels of p-STAT5
which appeared to localise to the nuclear membrane (Fig. 3D, E).
Similar to p.T352M and p.V325Wfs*26 variants, NanoBit com-
plementation assays demonstrated disrupted interactions between
p.F474del and WT-STAT5B (Fig. 3F). The missense variant (p.D574Y)
occurring in trans with p.P474del, and the compound heterozygous
variants in proband 5 showed reduced expression upon immuno-
blotting and immunofluorescence, when compared to wild-type (WT)

QSOX2 (Supplementary Fig. 3A, B). Similar to other characterised
variants, STAT5 phosphorylation was unaltered in response to GH, but
nuclear localisation was attenuated, and mutant interaction with WT-
STAT5B was markedly reduced (Supplementary Fig. 3C–F).

In silico modelling of QSOX2 supports STAT5B interaction
To better understand QSOX2-STAT5B interactions at the molecular
level, we utilised in silico modelling analyses. The domain boundary
predictions of QSOX2 according to IntFOLD7 are shown in Supple-
mentary Fig. 4A, with the sulfhydryl oxidase domain accentuated.
According to the PINOT server, STAT5B was shown to be a likely
interaction partner of QSOX2 binding to the sulfhydryl oxidase
domain, corroborating in vitro data (Supplementary Fig. 4B). Machine
learning algorithm, DISOPRED indicated long disordered and protein
binding regions at the N and C-termini of QSOX2 and the MEMSAT-SVM pre-
diction showed a membrane helix at the C-terminus (residues 658–683).

The potential MultiFOLD structure models of QSOX2 with the
locations of key mutated residues in the homodimer are shown in
Supplementary Fig. 4C. The p.K294R variant occurs in a domain linker
region between the first two domains, thus it may impact the relative
orientation of those domains. The p.V325Wfs*26 frameshift variant
results in complete loss of the sulfhydryl oxidase structural domain of
QSOX2. This likely leads to a loss of interaction with STAT5B and the
membrane-spanning helix (658–683), and a weakened homodimer
interaction. Amino acid residue 474 occurs in the FAD binding site,
therefore the p.F474del variant would likely disrupt the function of the
sulfhydryl oxidase domain (Supplementary Fig. 4D, E). The other var-
iants within the sulfhydryl oxidase domain of QSOX2 (p.T352M and
p.D574Y) may also affect the local domain structure and/or binding of
QSOX2 to STAT5B. Finally, the p.R683Q mutation occurs in the
C-terminal transmembrane spanning helix of QSOX2, therefore this
variant may affect membrane interaction.

Patient fibroblasts demonstrate aberrant STAT5B activity
We next assessed whether STAT5B dysregulation would be observed in
patient tissue. Patient-derived dermal fibroblasts were procured from
P2 and parents, with consent. P2 fibroblasts were noted to have neg-
ligible full-length QSOX2 expression when compared to parental (M, F)
and control (C) fibroblasts (Supplementary Fig. 2C, Fig. 4A). Similar to
in vitro reconstitution studies, P2 cells demonstrated enhanced GH-
induced STAT5B phosphorylation, nuclear sparing and cytoplasmic
accumulation (Fig. 4B, C). Interestingly, when cells were treated with
IGF-1, IGF-1-induced unequivocal phosphorylation of AKT and ERK in
control, P2 and parental fibroblasts confirming the impacts of QSOX2
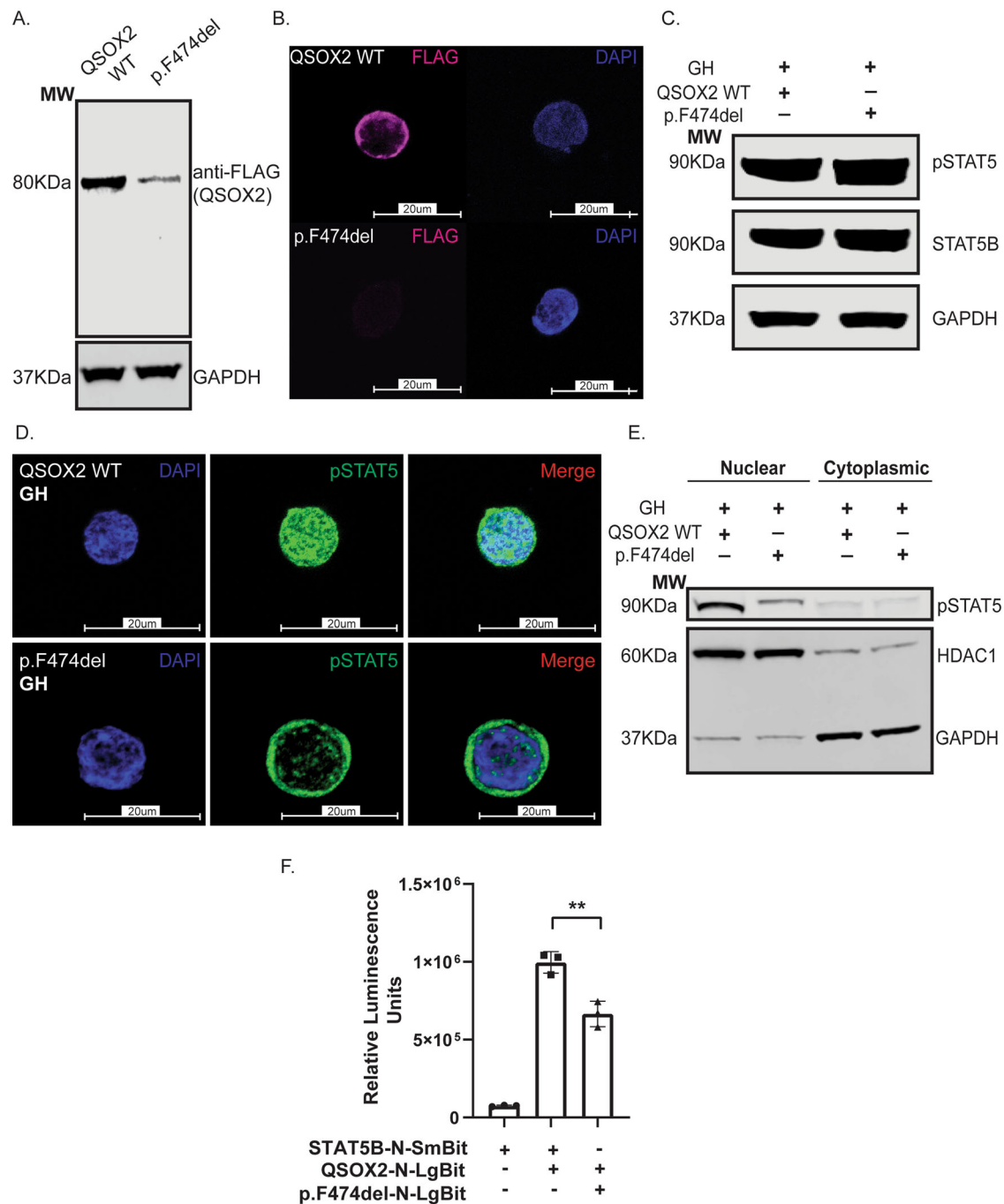deficiency precede *IGF1* transcription (Fig. 4D).

Fig. 3 | QSOX2 p.F474del variant function analogous to p.T352M and p.V325Wfs*26. A Expression of p.F474del was reduced compared to wild-type (WT)-QSOX2. Molecular weights (MW), in kiloDaltons, indicated left of the immunoblot. **B** Immunofluorescent microscopy demonstrated a reduction in QSOX2 peri-nuclear expression when compared to WT-QSOX2. **C** Immunoblot analyses of transfected HEK 293-hGHR cell lysates showed that in the presence of p.F474del, STAT5 was robustly phosphorylated following GH stimulation.
D Immunofluorescent microscopic analysis of GH-stimulated transfected HEK 293-hGHR cells revealed nuclear translocation impairment of p-STAT5 and perinuclear accumulation for p.F474del when compared to WT-QSOX2. **E** Nuclear and cytoplasmic fractionation of transfected HEK 293-hGHR cells were probed by immunoblotting for p-STAT5, nuclear marker HDAC1, and cytoplasmic GAPDH. A reduction of p-STAT5 in p.F474del nuclear fractions was noted when compared to wild type. **F** NanoBit complementation assays demonstrated blunted interaction between unstimulated STAT5B and QSOX2 p.F474del ($p = 0.0019$). Ordinary one-way-ANOVA was used for statistical analysis with multiple testing corrections performed using Sidak's test. Source data are provided as a Source Data file. Data are presented as the mean ± SD of three repeated measurements (3 independent replicates).

Mitochondrial dysfunction induced by GH in QSOX2 null cells

Recent studies have implicated STAT5 in mitochondrial gene expression, acting as both activator and repressor[24,25]. We, therefore, investigated the effect of enhanced GH-induced p-STAT5 on mitochondrial architecture. When compared to control and parental fibroblasts, confocal microscopy showed markedly fragmented mitochondria in P2 fibroblasts only following GH, but not when untreated or following IGF-1 stimulation (Fig. 4E). A concomitant increase in phospho-Ser616-DRP1 (Dynamin-related protein 1), a pro-fission marker of mitochondrial fragmentation, was observed (Fig. 4F). Increased cytoplasmic
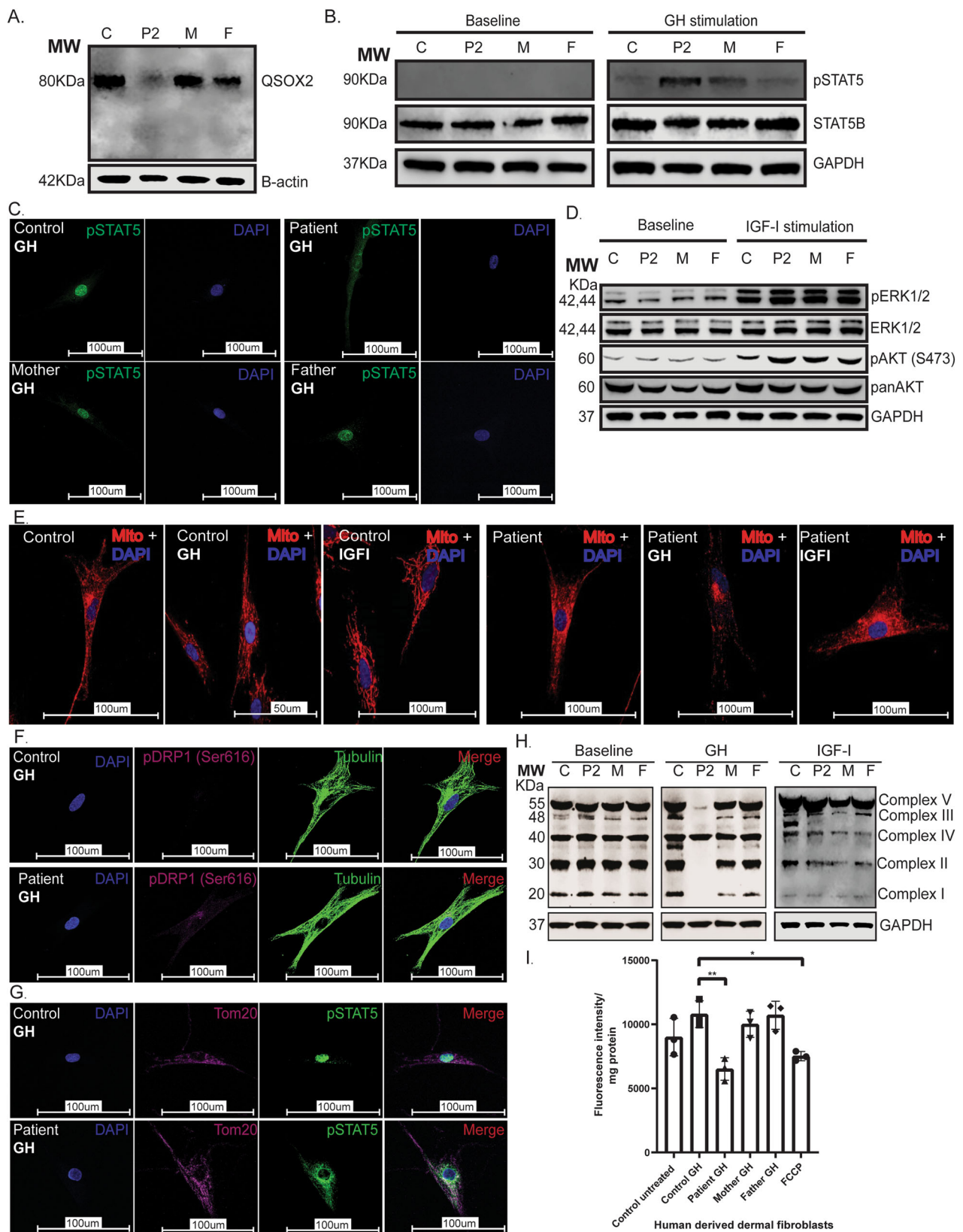
p-STAT5 in P2 fibroblasts co-localised to the mitochondrial outer membrane suggesting that in the absence of functional QSOX2, p-STAT5 may impact mitochondrial fragmentation via enhanced DRP1-S616 phosphorylation[26] (Fig. 4G). Profiling of electron transport chain complexes revealed a remarkable reduction of all complexes, except complex IV (Fig. 4H), which correlated with significant reductions in

mitochondrial membrane potential (Fig. 4I), solely in P2 fibroblasts and only after GH provocation.

The role of QSOX2 in GH signalling was further supported by a targeted *QSOX2* knockout human chondrocyte cell line which recapitulated the GH-mediated impact on STAT5B phosphorylation and mitochondriopathy (Supplementary Fig. 2D–G).

Fig. 4 | QSOX2 deficient patient (P2) dermal fibroblasts demonstrate STAT5B nuclear localisation defects and distinct mitochondrial dysfunction.
A Immunoblot analysis of control (C), proband 2 (P2) and parental dermal fibroblasts (M, F) revealed a global reduction in QSOX2 protein in patient-derived fibroblasts. **B** Robust tyrosine phosphorylation of STAT5 was elicited in patient fibroblasts when compared to control and heterozygote parents.
C Immunofluorescent microscopy indicated GH-stimulated p-STAT5 translocated to the nucleus in (C), M and F fibroblasts but not in P2 fibroblasts. P2 fibroblasts demonstrated diffused cytoplasmic staining for p-STAT5 with nuclear sparing.
D Immunoblot analysis of IGF-1 stimulated (100 ng/ml, 30 min) signalling pathways. IGF-1 activated pAKT, and pERK1/2 was comparable between P2, C and parental fibroblasts. **E** MitoTracker immunostaining of patient P2 fibroblasts, compared to control fibroblasts, indicate disrupted mitochondrial morphology upon GH, but not IGF-1, stimulation. Alterations in patient mitochondrial morphology seen with GH stimulation were consistent with mitochondrial fragmentation.
F Immunofluorescent microscopy of P2 fibroblasts demonstrated an increase in GH-induced phospho-S616-DRP1 when compared to control (C). **G** Cytoplasmic

accumulated p-STAT5B appeared to localise to the mitochondria in P2 fibroblasts co-immunostained for outer mitochondrial membrane marker, Tom20 and p-STAT5B. **H** Unstimulated and GH stimulated control (C), patient (P2), and parental (M, F) fibroblasts were immunoblot analysed for expression of mitochondrial oxidative phosphorylation complexes I–V. In P2 fibroblasts, a stark reduction in complex profiles was observed upon GH stimulation. IGF-1 stimulation, in contrast, did not alter complex profiles. **I** Mitochondrial membrane potential measurements of untreated and GH-treated primary fibroblasts with carbonyl cyanide p-tri-flouromethoxyphenylhydrazone, FCCP (20 μM) added to control fibroblasts as a depolarisation control. Reproducible reduction in mitochondrial membrane potential was detected in GH-treated patient fibroblasts compared to control fibroblasts ($p = 0.0013$). FCCP depolarisation control effectively showed reduced mitochondrial membrane potential when compared to GH-treated control fibroblasts ($p = 0.0105$). Ordinary one-way-ANOVA was used for statistical analysis with multiple testing corrections performed using Sidak's test. Source data are provided as a Source Data file. Data are presented as the mean ± SD of three repeated measurements (3 independent replicates).

Discussion

We present three families with autosomal recessive QSOX2 deficiency, characterised by a distinct phenotypic spectrum including significant postnatal growth restriction, feeding difficulties, eczema, gastrointestinal dysmotility and mild immunodeficiency. The identified *QSOX2* variants were associated with attenuated STAT5B nuclear localisation. Simultaneously, increased GH-induced cytosolic accumulation of p-STAT5 in dermal fibroblasts correlated with disrupted mitochondrial morphology suggesting potential inter-organelle dysfunction. Hence, we uncovered biologically distinct functions for QSOX2, which, when lost, results in a complex disorder.

Population-based data implicate *QSOX2* as a height-associated locus with several polymorphisms (GRCh38 genome build) (9:136227369_A/G, 9:136220024_G/T and 9:136229894_A/C,T) identified as adult height determinants[13,27,28]. Interestingly, genetic association analysis of homozygous missense variant SNP rs61744120 (*c.1055 C > T*, p.T352M), enriched in the Finnish population (the Finnish THL Biobank), identified a significant inverse association with adult height. Discernible differences, however, were noted amongst the 16 validated homozygotes. We postulated, based on in vitro assays and detection of exon 8 skipping in mRNA transcripts from patient (P2) fibroblasts, that the SNP may give rise to a predicted missense variant as well as a mis-spliced exon skipped transcript. Expression of this alternatively spliced transcript may be largely tissue-specific or relegated to disease states[29]. Indeed, a mistranslation of the p.T352M protein in humans may produce unintended consequences, where identical genotypes may produce phenotypic variance even at the tissue level due to stochastic gene expression. Altogether, transcript heterogeneity, different genetic backgrounds in *c.1055 C > T* homozygotes, variable penetrance and variable expressivity can all account for imperfect phenotype-genotype correlations[30,31].

Given the pleiotropic nature of this disorder, phenotypic variability was inevitably anticipated. The degree of short stature appeared most pronounced in compound heterozygotes (4/5 probands) when compared to the lone simple recessive homozygote (P3) within our cohort. Since the impact of p.T352M homozygosity on height is highly variable, it seemed possible that phenotypic discordance may be due to interallellic complementation[32,33]. The QSOX2 protein may have altered functionality or negative interallelic complementation between two distinct mutants in trans as opposed to identical mutant subunits, which may have the unintended consequence of partial phenotypic rescue or positive interallelic complementation i.e., the heteromultimer is less functionally active than the homomultimer.

All clinically associated *QSOX2* variants evaluated demonstrated strikingly attenuated nuclear localisation of STAT5B with preservation of both GH-mediated phosphorylation and dimerisation, akin to the

translocation defect of the known STAT5B p.Q177P. This latter variant is located in the CCD, a module critical for nuclear localisation[4]. The reduced affinity of STAT5B p.Q177P for QSOX2 implies that the CCD module may be involved in QSOX2 binding. Collectively, our data support nuclear membrane QSOX2 as an interactor directing the nuclear import of STAT5B, a process integral for *IGF1* transcriptional regulation. These findings are consistent with low serum IGF-1 in P1, P2 and P5.

Altered STAT5B activity is ubiquitously associated with maladaptive immune signalling. Congenital dominant negative and loss of function *STAT5B* variants give rise to a wide phenotypic spectrum ranging from mild eczema to autoimmune disease that can potentially lead to fatal pulmonary fibrosis and respiratory failure[7]. Unlike endocrine profiles, which show an absolute association between loss-of-function *STAT5B* variants and IGF-1 deficiency, abnormalities in immunological profiles are often variable, even between siblings carrying the same pathological homozygous *STAT5B* variant[34,35]. Indeed, since many cytokines activate STAT5B, impacts on immunity are expected. For example, a syndrome of surfactant accumulation due to dysregulated GM-CSF signalling in alveolar macrophages, with features of lymphocytosis, bronchiectasis and fibrosis, was associated with a homozygous frameshift *STAT5B c.1680delG* variant[8]. Other reports of STAT5B-associated immune deficiencies due to cytokine dysregulation include pronounced T-cell lymphopenia, altered NK cell maturation, and impaired humoral immune dysregulation[17,35–38]. Intriguingly, a previously reported autosomal recessive *STAT5B c.1102insC* truncating variant[5,39] and a recently reported truncating variant, *c.1453delG*[40], were both associated with relatively normal immune profiles lacking the severe immune deficiency typically associated with loss of function *STAT5B* defects. It is of note that somatic gain of function *STAT5B* variants are associated with allergic inflammation and large granular cell leukaemia[9]. Collectively, the link between STAT5B and immune function appears inextricable, but still mechanistically not well understood.

In our cohort, growth failure is universal, and while the patients have variable presentations of altered immunity, eczema appears to be a highly penetrant feature, similar to patients with STAT5B deficiency[4]. Although the downstream impact of attenuated STAT5B nuclear localisation contributed to the phenotypes, the association of immunodeficiency and gastrointestinal dysfunction with loss of *QSOX2* prompted an investigation into interferon signalling given overlap with excessive interferon states such as APECED[41]. However, an interferon (IFN) signature gene assay conducted on probands 1, 2 and 5 revealed no evidence of interferonopathy in peripheral blood samples. Interestingly, a concordant downregulation of SIGLEC1 (sialic acid binding Ig like lectin 1) was of note in P1 and P2. SIGLEC1 is a key

regulator of phagocytic function, and its deficiency is implicated in the pathogenesis of obstructive pulmonary disease[42]. IFI27, elevated in P5, is a pro-apoptotic protein present at the mitochondrial membrane and implicated in IFN-dependent modulation of mitochondrial permeability[43]. Further work is necessary to characterise these findings in the context of QSOX2 insufficiency.

The striking mitochondrial dysregulation induced by GH has not been previously reported. Mitochondrial disruption was observed in both our *QSOX2* knock-out gene-edited C28/I2 chondrocytes and in patient fibroblasts. The induction of mitochondrial fragmentation, dramatic reduction in detectable oxidative phosphorylation complexes and decreased mitochondrial membrane potential were only noted after GH stimulation. Whether these effects were a direct consequence of increased cytoplasmic p-STAT5 remains to be fully determined. Notably, both tyrosine phosphorylated and unphosphorylated forms of STAT5A/B have been reported to translocate to the mitochondria and disrupt the pyruvate dehydrogenase complex (PDC), leading to altered mitochondrial function, decreased membrane potential and overall reductions in mitochondrial proteome quality control[44,45].

Cytokine-activated STAT5 has also been shown to reduce mitochondrial DNA expression by binding to the D-loop leading to attenuation of the electron transport chain[24,25]. Global reorganisation of oxidative phosphorylation complexes and significantly attenuated mitochondrial membrane potential in our QSOX2-deficient fibroblasts suggest a definitive impact on mitochondrial metabolism. In neurons, Interferon-β (IFN-β) stimulation leads to mitochondrial localisation of phosphorylated STAT5, which induces phospho-S616-DRP1 via upregulation of PGAM5 phosphatase, thereby promoting mitochondrial fission[26]. In the QSOX2 deficient fibroblasts, the striking detection of phospho-S616-DRP1 is consistent with an abundance of GH-stimulated cytoplasmic tyrosine phosphorylated STAT5B. Overall, our findings suggest a definitive impact of QSOX2 deficiency on mitochondrial metabolism, possibly involving STAT5B.

Disorders of mitochondrial DNA are often characterised by altered gastrointestinal sensorimotor kinetics[46]. Interestingly, all *QSOX2* deficient patients presented with gastrointestinal (GI) manifestations, the cumulative effect of which may be due, in part, to dysregulated STAT5B signalling on mitochondrial dynamics, although a distinct role for QSOX2 in GI tract physiology remains to be elucidated. The possibility of GI manifestations contributing to growth impairment in our QSOX2 deficient patients cannot be entirely discounted, although optimisation of nutrition/PEG feeding in P1 and P2 did not result in catch-up growth.

Despite functional evidence that GH exerts disruptive effects in QSOX2 deficiency, a 2.0-year regime of recombinant-GH normalised serum IGF-1 and promoted modest increases in growth velocity in both P1 and P2. GI symptoms, however, did not improve with GH therapy. Interestingly, murine studies have demonstrated an intestinotropic effect of IGF-1, independent of GH, which positively regulates intestinal growth and physiology[47]. We hypothesise that tissue-specific deficiency of IGF-1 may, in part, account for disease pathogenesis and as demonstrated in other partial GHI patients, initiation of rhIGF-1 therapy alone or in combination with rhGH in our patients may be able to induce accelerated/sustainable growth and improve other symptoms[3,18,48].

In summary, we describe a multi-system disorder (Maharaj Storr Syndrome), QSOX2 deficiency, which should be suspected in individuals with atypical GHI, low IGF-1 and prominent immune/gastrointestinal dysregulation. Therapeutic recombinant IGF-1 may potentially circumvent the GH-mediated STAT5B molecular defect and potentially alleviate organ-specific disease. We describe the executive functions of QSOX2, located at the nuclear membrane, namely acting as a "gatekeeper" for regulating the import of p-STAT5B and important for mitochondrial integrity. Ongoing and future work includes monitoring the young probands and advancing the understanding of cellular mechanisms involved in QSOX2 deficiency.

Methods

Ethical approval
Informed written consents for genetic research, derivation of dermal fibroblasts and publication of clinical details, including indirect identifiers, were obtained from human research participants and their guardians. Participants consented to the publication of anonymised clinical data in an open-access journal and were not compensated for the study. The study was approved by the Health Research Authority, East of England-Cambridge East Research Ethics Committee (REC reference 17/EE/0178).

Antibodies and probes
Rabbit anti-QSOX2 antibody (ab121376, RRID:AB_11128050, dilution 1:1000), Monoclonal ANTI-FLAG® M2 antibody (Sigma Aldrich F3165, RRID:AB_259529, dilution 1:1000), Rabbit anti-Phospho-Stat5 antibody (Tyr694) (Cell Signalling Technology D47E7, RRID:AB_10544692, dilution 1:500), Rabbit anti-phospho-Stat3 antibody (Tyr705) (Cell Signalling Technology D3A7, RRID:AB_2491009, dilution 1:500), Rabbit anti-phospho-Stat1 antibody (Tyr701) (Cell Signalling Technology Clone 58D6, RRID:AB_561284, dilution 1:500), Rabbit anti-Tom20 antibody (Cell Signalling Technology D8T4N, RRID:AB_2687663, dilution 1:200), Rabbit anti-phospho-DRP1 (Ser616) (Cell Signalling Technology D9A1, RRID:AB_11178659, dilution 1:200), Rabbit anti-GAPDH antibody (ab9485, RRID:AB_307275, dilution 1:10,000), Mouse anti-Actin beta monoclonal antibody (ab6276, RRID:AB_2223210, dilution 1:10,000), Mouse anti-Histone Deacetylase 1 antibody (Santa-Cruz biotechnology sc-81598, RRID:AB_2118083, dilution 1:1000), Rabbit anti-GFP antibody (ab290, RRID:AB_303395, dilution 1:1000), Fluorescent probe - Mito-Tracker™ Red (M22425, Thermo Fisher Scientific), Rat anti-Human phospho-STAT5a/b Y694/Y699 (R&D Systems Clone MAB4190, dilution 1:300), Mouse anti-alpha Tubulin antibody DM1A (ab7291, RRID:AB_2241126, dilution 1:1000), Total OXPHOS Rodent WB Antibody Cocktail (ab110413, RRID:AB_2629281, dilution 1:500), Rabbit anti-Phospho-Akt (Ser473) antibody (Cell Signalling Technology D9E, RRID:AB_2315049, dilution 1:750), Rabbit anti-Akt (pan) antibody (Cell Signalling Technology C67E7, RRID:AB_915783, dilution 1:1000), Rabbit anti-MAP Kinase (ERK-1, ERK-2) antibody (Sigma Aldrich M5670, RRID:AB_477216, dilution 1:1000), Monoclonal anti-MAP Kinase, Activated (Diphosphorylated ERK-1&2) antibody (Sigma Aldrich M9692, RRID:AB_260729, dilution 1:1000), Goat anti-Rat IgG (H + L) Highly Cross-Adsorbed Secondary Antibody Alexa Fluor Plus 488 (A48262 RRID:AB_2896330, dilution 1:500), Goat anti-mouse IgG (H + L) Highly Cross-Adsorbed Secondary Antibody Alexa Fluor Plus 488 (A32723, RRID:AB_2633275, dilution 1:500), Goat anti-Rabbit IgG (H + L) Highly Cross-Adsorbed Secondary Antibody, Alexa Fluor Plus 647 (A32733, RRID:AB_2633282, dilution 1:500), IRDye® 800CW Goat anti-Mouse IgG (RRID:AB_10793856, dilution 1:5000), IRDye® 800CW Goat anti-Rabbit IgG (RRID:AB_10796098, dilution 1:5000), IRDye® 680RD Goat anti-Mouse IgG (RRID:AB_2651128, dilution 1:5000), IRDye® 680RD Goat anti-Rabbit IgG (RRID:AB_2721181, dilution 1:5000), Tetramethylrhodamine, ethyl ester (TMRE, ab113852).

Variant prioritisation and top genomic candidates
Whole exome sequencing of Probands 1 and 2 was conducted by the Otogenetics Corporation using an Illumina HiSeq 2500 platform. Downstream analysis was conducted using Ingenuity variant analysis (https://variants.ingenuity.com/qci/). Variants with a call quality ≥ 20 were retained, whilst common variants with an allele frequency ≥ 0.5% in databases such as gnomAD, ExAC, NHLBI ESP and 1000 genomes project were excluded unless designated as known disease-causing variants. Deep intronic variants (> 20 bp into the intron), and those predicted to be pathogenic, likely pathogenic or variants of uncertain

significance as computed by ACMG guidelines were kept. Variants associated with gain of function as well as loss of function frameshift, indel, missense, nullizygous, splice site (up to 20 bases into intron), copy number loss and deleterious to a microRNA were retained. Variants that were homozygous, heterozygous, heterozygous_ambiguous and homozygous in both probands were prioritised. Using a recessive disease model, the top candidates were the compound heterozygous variants found in *QSOX2*. Other top candidates, which were not consistent with phenotypes, are summarised in Supplementary Table 4.

QSOX2 Variant detection and confirmation

Variants in *QSOX2* were confirmed by Sanger sequencing using primers amplifying exon 8 (forward: 5′-CCAGGACAGGGAGACTTG-3′ and reverse: 5′-GGTGGAGAGCACCTCAG-3′), exon 10 (forward: 5′-CCCAGTCAAGAAGGCAG-3′ and reverse: 5′-AGTACATGCCTTTGCA-CAC-3′) and exon 12 (forward: 5′-GAGTGGGAGTCCGGTTG-3′ and reverse: 5′-CATCCGATGTGAAACCAG-3′) of *QSOX2*. Pathogenicity of both variants was evaluated using a combination of predictive tools: Sorting Intolerant from Tolerant, Polymorphism Phenotyping v2, Combined Annotation Dependent Depletion and Mutation taster.

Protein structure modelling and thermostability analysis

Protein 3D modelling of the Alpha Fold Protein Structure Database[49] QSOX2 crystal structure Q6ZRP7 was performed using the tool PyMOL (Schrodinger, LLC. 2010. The PyMOL Molecular Graphics System, Version 2.3.3, https://pymol.org/2/) with thermostability of the missense mutant protein assessed using computational platforms: DynaMut[50], I-Mutant[51], SDM[52], DUET[53], MUpro_SVM[54] and mCSM[55]. QSOX2 was modelled using the IntFOLD7 and MultiFOLD servers[56]. QSOX2 domain boundary locations and protein-ligand interactions were modelled using the IntFOLD7 server. The PINOT[57] server was used to verify interaction partners of QSOX2. The DISOPRED3[58] server was used to predict disordered and protein-binding regions, and MEMSAT-SVM[59] was used to identify membrane-spanning regions in QSOX2.

UK Biobank (UKBB) data analysis

We included 420,162 samples of European ancestry in the UKBB for exome-wide association tests. For the 450 K release of exome-sequencing data in the UKBB, we performed individual and variant-level quality control procedures previously described by Gardner et al.[60]. Variants were annotated using ENSEMBL Variant Effect Predictor (VEP) v104[61]. Protein truncating variants were defined as stop gain, frameshift, splice acceptor and splice donor variants. The burden test assumed the presence or absence of variants of interest in a gene as an indicator variable, which was regressed against the phenotype in a linear mixed model using BOLT-LMM v2.3.6[62] on the UKBB Research Analysis Platform (RAP). Covariates adjusted in the burden test included age at assessment (UKBB Data-field 21003), age squared, the whole-exome sequencing batches (as a categorical variable, either 50, 200, or 450 K) and the first 10 genetic principal components (UKBB Data-field 22009.1-10).

Quality check for rs61744120 imputation and data analysis

To study the quality of the imputed SNP rs61744120, we compared the genotypes between WGS and FinnGen imputed data in FINRISK participants where data was available for both formats. The FINRISK cohorts comprise the respondents of representative, cross-sectional population surveys that have been carried out every 5 years since 1972 (to assess the risk factors of chronic diseases and health behaviour in the working-age population) in 3-5 large study areas of Finland. THL Biobank host samples were collected in the following survey years: 1992, 1997, 2002, 2007, and 2012. Genome-wide imputation was done as part of the FinnGen project using Sequencing Initiative Suomi (SISu) project data as a reference.

Individuals with the minor/minor genotype were identical between WGS and both releases of the imputed data. However, there were variations in minor/major and major/major genotypes in 10 individuals producing an error rate of 0.25%. The additive genetic association model was utilised to estimate the proportional risk of disease i.e., reduction in height associated with this single nucleotide polymorphism. Calculation of height standard deviation scores based on raw height data of minor/minor homozygotes was performed using Finnish population-based references for healthy subjects as outlined by Saari et al.[63].

In vitro splicing assay

An in vitro splicing assay was designed, as previously described by Maharaj et al.[64], using the Exontrap vector pET01 (MoBiTec). A designated DNA sequence, including exons 7 and 8 of *QSOX2* as well as intervening introns, was selectively cloned into the multiple cloning site of the exon trap splicing machinery. Clones were selected and verified by sanger sequencing using vector-specific primers ET 06 (forward: 5′-GCGAAGTGGAGGATCCACAAG-3′) and ET 07 (reverse: 5′-ACCCGGATCCAGTTGTGCCA-3′). Site-directed mutagenesis to generate the *c.1055 C > T* (p.T352M) variant was performed using the QuikChange II XL site-directed mutagenesis kit (Agilent, 200521) according to the manufacturer's instructions. Empty pET01 vector, *QSOX2*-WT and variant clones were transfected into mammalian HEK293 cells for 24 h, followed by RNA extraction. cDNA synthesis was performed using the vector-specific hexamer GATCCACGATGC and RT-PCR conducted using pET01 primer 02 (forward: 5′-GAGG-GATCCGCTTCCTGGCCC-3′) and primer 03 (reverse: 5′-CTCCCGGGCCACCTCCAGTGCC-3′). PCR products were analysed on a 2% agarose gel and bands gel extracted, column purified and confirmed by Sanger sequencing.

RNA isolation and cDNA synthesis

RNA was extracted from control and patient fibroblasts using the RNeasy mini kit (Qiagen, 74134) according to the manufacturer's instructions. Genomic DNA removal was performed using an RNase-Free DNase Set (Qiagen, 79254). For cDNA synthesis, 1 μg of RNA (with 10 mM random hexamer and nuclease-free water to a volume of 15 μL) was incubated at 70 °C for 5 min. MuMLV reverse transcriptase enzyme and 10X buffer, RNase Inhibitor and dNTP were then added to the reaction and placed on a thermo-cycler at 25 °C for 10 min, 42 °C for 90 min and 70 °C for 15 min.

RT-PCR

RT-PCR was performed using cDNA primers spanning exons 7 to 9 of *QSOX2* (Exon 7 Forward 5′-CTTCCCTTGCCTGAAAAG-3′ and Exon 9 Reverse 5′-CGTTGTAGGGGATCCTG-3′). The reaction mixture contained a 20 ng cDNA template, 1 × Standard Taq Buffer, 10 nM for each deoxyribonucleotide triphosphate (dNTP), 100 μM for each primer, and 40U *Taq polymerase* (NEB). Thermocycling conditions: 95 °C for 5 min, 10 x (95 °C for 30 sec, 65 °C for 30 sec (−1 °C per cycle), 72 °C for 30 sec), 25 x (95 °C for 30 sec, 55 °C for 30 sec, 72 °C for 30 sec), 72 °C for 5 min and storage at 4 °C until further processing. Products were run on a 1.5% agarose gel and resolved by electrophoresis at 100 V for 80 min. Fluorescent bands were gel extracted and purified using the Macherey Nagel-NucleoSpin Gel and PCR Clean-up kit according to manufacturer's instructions, and products were sequenced (Sanger sequencing).

Site-directed mutagenesis

Site-directed mutagenesis of a QSOX2 (NM_181701.4) Human Tagged ORF Clone (GenScript, ID: OHu07590C) was performed using the QuikChange II XL site-directed mutagenesis kit (Agilent, 200521) according to the manufacturer's instructions. Primers for the generation of *QSOX2* variants were designed using the online tool https://www.agilent.com/store/primerDesignProgram.jsp. Primers are listed

as follows: p.T352M (Forward 5′-GTCCTTGAGCATCTTCAGCTCTGCTC CGG-3′ and Reverse 5′-CCGGAGCAGAGCTGAAGATGCTCAAGGAC-3′), p.V325Wfs*26 (Forward 5′-CTGACTCCAGGTCCACGTGTACAGCTTC GA-3′ and Reverse 5′-TCGAAGCTGTACACGTGGACCTGGAGTCAG-3′), p.F474del (Forward 5′-GAGGAGGTACGTTCACACCTTTGGGTGTAAG G-3′ and Reverse 5′-CCTTACACCCAAAGGTGTGAACGTACCTCCTC-3′), p.K294R (Forward 5′-GCAAGGGAAGCGATTTTCTCCTCACATCCGGC AAT-3′ and Reverse 5′-ATTGCCGGATGTGAGGAGAAAATCGCTTCCC TTGC-3′) and p.R683Q (Forward 5′-CGCCTGGACCTCACCTGGAAGAA GAAGTACA-3′ and Reverse 5′-TGTACTTCTTCTTCCAGGTGAGGTCC AGGCG-3′).

Primary fibroblast cell culture

Fibroblast isolation was performed from skin punch biopsies of proband 2, parents and a healthy control. Immediately after excision, the specimen was incubated in DMEM high glucose supplemented with 10% Foetal Bovine Serum (FBS) and 1% Penicillin/Streptomycin. The skin specimen, chopped into 1 mm cubes, was subsequently digested using a mixture of nutrient media (DMEM high glucose supplemented with 10% FBS, 1% penicillin/streptomycin and 1:100 non-essential amino acids), 0.25% collagenase and 0.05% DnaseI. The mixture, incubated at 37 °C in 5% CO_2 overnight, was centrifuged at 1000xg for 5 min, and the pellet resuspended in fibroblast primary culture media (DMEM high glucose with 10 % FBS, 1% penicillin/streptomycin and 1:100 non-essential amino acids). The resuspended mixture was plated in a 0.1% gelatin-coated T25 flask and left in an incubator at 37 °C in 5% CO_2 until fibroblast cultures were established.

Cell culture, GH/IGF-1 stimulation and nuclear fractionation

Dermal fibroblasts and C28/I2 chondrocytes were cultured in DMEM high glucose supplemented with 10% FBS and 1% penicillin/streptomycin. HEK 293-hGHR cells[65] were similarly cultured in DMEM high glucose base media with selection antibiotic, G-418 (Sigma Aldrich), at a concentration of 400 μg/ml. Prior to GH treatment, cells were serum-deprived for at least 24 hours in serum-free media supplemented with 0.1% Bovine serum albumin (BSA). Optimal standardised human GH (Cell Guidance Systems) concentration (500 ng/ml) was used for all experiments with a stimulation time of 20 min at 37 °C in 5% CO_2. For IGF-1 stimulation, cells were similarly serum-deprived for 24 h prior to treatment with recombinant human IGF-1 (Peprotech, 100 ng/ml) for 30 min at 37 °C in 5% CO_2. Nuclear and cytoplasmic cell fractions were prepared using the NE-PER™ Nuclear and Cytoplasmic Extraction Reagents (Thermo Fisher) according to the manufacturer's instructions. Cross-contamination of cellular fractions was negligible.

CRISPR-Cas9 Engineered Knockout of *QSOX2* in C28/I2 Human Chondrocyte Cell Line

CRISPR gene editing was achieved by utilising the protocol outlined by Ran et al.[66]. Guide sequences were designed using the online CRISPR Design Tool (http://tools.genome-engineering.org). The single guide RNA oligos (Forward 5′-GGGACCTGCGCTGAGAG-3′ and Reverse 5′-GCGGTAAGGAAAGAAATACGG-3′) were then cloned into pSpCas9(BB)-2A-GFP (PX458), a gift from Feng Zhang (Addgene plasmid #48138; http://n2t.net/addgene:48138; RRID:Addgene_48138, https://www.addgene.org/48138)[66] and introduced into immortalised C28/I2 (Sigma Aldrich™, Catalogue no. SCC043) human chondrocyte cells via transfection using Lipofectamine™ 3000 according to manufacturer's instructions. After 72 h, GFP-positive cells were cell sorted by fluorescence-activated cell sorting into prepared 96-well plates to ensure single-cell clonal expansion. Colonies were expanded and genotyped after 4 to 6 weeks.

Co-immunoprecipitation

In order to probe the interaction between QSOX2 and endogenous STAT5B, 7 μg of QSOX2 cDNA was transfected into 2×10^6 HEK 293-

hGHR cells (10 cm dish) using Lipofectamine™ 3000 according to manufacturer's instructions. After 48 h, cells were lysed with 0.5% NP-40 buffer (0.5% NP-40, 20 mM Tris–HCl, 150 mM NaCl, 1 mM EDTA, 10% glycerol, 1 mM PMSF). The lysate was added to a micro-centrifuge tube, placed on a rotary mixer for 1 h at 4 °C, and then centrifuged for 20 min at $14,000 \times g$. Protein concentration was quantified using a Bradford protein assay (Bio-Rad). Lysate was equally divided into three separate micro-centrifuge tubes, and Immunoprecipitation was carried out at 4 °C overnight following the addition of primary antibodies (5 μg anti-STAT5B, 5 μg anti-QSOX2 and 5 μg Goat anti-mouse IgG - H&L - Fab Fragment Polyclonal Antibodies) and Protein G Sepharose beads (Sigma-Aldrich). Bound proteins were extracted from coated beads and analysed by immunoblotting.

Pull down assay

To assess whether the presence or absence of QSOX2 impacts the dimerisation of STAT5B, *QSOX2* wild type and knockout C28/I2 cells were transfected in parallel with pCMV6-AC-GFP-STAT5B and pCMV6-AC-STAT5B-FLAG plasmids using Lipofectamine™ 3000 according to manufacturer's instructions. After 12 h, complete media was removed, and cells were cultured in serum-free media supplemented with 0.1% BSA for a further 24 h. Cells were treated with GH 500 ng/ml for 20 min prior to the addition of lysis Buffer (50 mM Tris HCl, pH 7.4, with 150 mM NaCl, 1 mM EDTA, and 1% TritonX-100). Lysates were placed on a rotary mixer for 1 h at 4 °C prior to clarification by centrifugation at $14,000 \times g$ for 15 min. ANTI-FLAG M2-Agarose Affinity Gel beads (Sigma Aldrich) were equilibrated with TBS prior to the addition of protein samples and incubated at 4 °C overnight on a rotary mixer. Coated beads were collected and washed with TBS (twice). Samples were eluted using SDS sample buffer, separated by SDS-PAGE gel electrophoresis and probed by immunoblotting using monoclonal anti-FLAG and monoclonal anti-GFP antibodies.

Immunoblotting

Whole-cell lysates were prepared by the addition of RIPA buffer (Sigma Aldrich) supplemented with protease and phosphatase inhibitor tablets (Roche). Protein concentrations were quantified using a Bradford protein assay (Bio-Rad), and lysates were denatured by the addition of SDS sample buffer 6 × (Sigma Aldrich) and boiled for 5 min at 98 °C. A 20-μg bolus of protein was loaded into the wells of a 4% to 20% sodium dodecyl sulfate-polyacrylamide gel electrophoresis gel (Novex) prior to electrophoretic separation using MOPS buffer. Protein transfer to nitrocellulose membrane was achieved by electroblotting at 15 V for 45 min. The membrane was blocked with either 5% fat-free milk or BSA in tris-buffered saline/0.1% Tween-20 (TBST) and left to gently agitate for 1 h. Primary antibody was added at a concentration of 1:1000 with housekeeping control at a concentration of 1:10,000. Primary antibody incubation was left overnight at 4 °C with gentle agitation. The membrane was then washed for 5 min (3 times) with TBST. Secondary antibodies were added at a concentration of 1:5000 to the blocking buffer, and the membrane was incubated at 37 °C for 60 to 90 min. The membrane was subsequently washed 3 times (5 min each) with TBST and visualised with the LI-COR Image Studio software for immune-fluorescent detection.

Mitochondrial membrane potential assay

Fibroblasts were seeded in clear-bottomed 96 well plates (1×10^5 cells/well) and cultured at 37 °C in 5% CO_2 overnight. Culture medium was aspirated, replaced with serum-free base media supplemented with 0.1% BSA and cells incubated at 37 °C for a further 8 h. GH (500 ng/ml) and depolarisation control carbonilcyanide p-triflouromethoxyphenylhydrazone, FCCP (20 μM) were added to relevant wells and plate incubated at 37 °C in 5% CO_2 for 10 min. Tetramethylrhodamine ethyl ester (TMRE) was then added at a concentration of 500 nM and cells were incubated for a further

20 min at 37 °C in 5% CO_2. Media was aspirated from wells and replaced by 100 µl of PBS/0.2% BSA. This process was repeated prior to fluorescence measurement (Ex/Em = 549/575 nm) using the CLARIOstar Multimode Plate Reader (BMG Labtech).

GHRE Luciferase reporter assay

HEK 293-hGHR cells were seeded in six-well plates and transiently transfected with 2.5 µg DNA per well: 1.0 µg pGL2 8xGHRE (growth hormone response element) luciferase reporter plasmid, 0.5 µg STAT5B WT, 0.5 µg QSOX2 WT/mutant cDNA /empty vector and 0.5 µg pRL-SV40 (*Renilla* luciferase). After overnight incubation, the culture medium was replaced with serum-free DMEM supplemented with 0.1% BSA and incubated for a further 8 h. Cells were stimulated with GH (500 ng/ml) for 24 h and lysates collected and assayed using the Dual-Luciferase® Reporter Assay System (Promega, E1910) on the CLARIOstar Multimode Plate Reader (BMG Labtech).

Immunofluorescence

Cells seeded on glass coverslips (24 well plates) were fixed with 4% paraformaldehyde for 15 min. Cells were then washed three times in PBS and permeabilized in ice-cold 100% methanol for 10 min at −20 °C. After three further PBS washes, coverslips were incubated in Blocking buffer (1X PBS / 5% goat serum / 0.3% Triton™ X-100) at room temperature for 60 min. Primary antibody (rat anti-STAT5B, rabbit anti-QSOX2, rabbit anti-Tom20, rabbit anti-phospho-DRP1, mouse anti-alpha tubulin) reconstituted in dilution Buffer (1X PBS / 1% BSA / 0.3% Triton™ X-100 buffer) was added to cells and left at 4 °C overnight with gentle agitation. Cells were then washed three times with PBS prior to the addition of fluorescent secondary antibody and left at room temperature for 90 min (protected from light). Coverslips were counterstained with DAPI and washed with PBS to mount on microscope slides.

MitoTracker immunostaining

For MitoTracker staining of mitochondria, fibroblast and C28/I2 cells were seeded at a density of 2.5×10^3 per well (24 well plates) on glass coverslips. The MitoTracker lyophilised probe was reconstituted in anhydrous DMSO to a stock concentration of 1 mM. A working concentration of 100 nM was established by dilution in nutrient media prior to addition to cells and incubated at 37 °C in 5% CO_2 for 30 min. After incubation, cells were washed twice with phosphate-buffered saline (PBS) and coverslips fixed with 4% paraformaldehyde for 15 min. Permeabilization was achieved by the addition of 0.2% TritonX-100 for 5 min. Coverslips were counterstained with DAPI and washed with PBS to mount on microscope slides. Images were obtained using the 63x oil objective of the confocal Laser scanning microscope 710.

Generation of Nanoluc SmBiT and LgBiT (STAT5B-N-small BiT and QSOX2-N-Large BiT fusion vectors) by Gibson assembly

Wild-type STAT5B and QSOX2 constructs were generated by cloning Nanoluc small BiT (SmBiT) and large BiT (LgBiT) sequences to the N terminus of each receptor using a flexible Glycine-(gly)-Serine-(ser) linker by Gibson assembly. Primers were designed using the Benchling assembly wizard (Benchling Biology Software 2020, https://benchling.com). Constructs were generated following the Gibson assembly methodology according to the manufacturer's instructions (Gibson Assembly Master Mix, NEB®). A Phusion High-Fidelity PCR Kit (NEB®) was used to amplify target sequences. Thermocycling conditions were as follows: Denaturation at 98 °C for 3 min, amplification 35 x (98 °C for 30 sec and 72 °C for 20−30 sec/Kb) and elongation at 72 °C for 10 min. Gel electrophoresis was used to visualise products prior to *Dpn*I digestion. Fragments were ligated using NEBuilder® HiFi

DNA Assembly Master Mix (NEB®) and transformed using NEB® competent E. coli cells. Single colonies were selected for mini-preparation and accurate assembly of constructs verified by Sanger sequencing. *QSOX2* (p.T352M, p.V325Wfs*26, p.F474del) and *STAT5B* (p.Q177P) variant constructs were generated by site-directed mutagenesis as outlined above.

NanoBiT complementation assays

Protein-protein interactions were assessed with NanoBiT complementation assays using the STAT5B WT/mutant and QSOX2 WT/mutant plasmids N terminally fused with NanoBiT fragments (LgBiT and SmBiT). HEK 293-hGHR cells (1×10^5 cells/well) were seeded in poly-D-lysine coated white bottom 96-well plates, and plasmids were reverse-transfected using Lipofectamine™ 3000 according to the manufacturer's instructions. The optimal DNA concentration required for maximum bioluminescence signal was determined to be 200 ng per well; 100 ng SmBiT-STAT5B and 100 ng LgBiT-QSOX2. 24 h post-transfection, cell culture medium was removed and replaced with 100 µL NanoBiT assay buffer (pH 7.4, HBSS 1X, HEPES 24 mM, NaHCO$_3$ 3.96 mM, CaCl$_2$ 1.3 mM, MgSO$_4$ 1 mM, BSA 0.1%) per well and equilibrated for 1 h at 37 °C in 5% CO_2. Following equilibration, six (6) baseline luminescence readings were recorded using the CLARIOstar Multimode Plate Reader (BMG Labtech). Furimazine (Nanolight Technology) was prepared in a 1:50 dilution with assay buffer, and 25 µl was added to each following baseline measurements, and readings continued for 1 h.

Statistics and reproducibility

No statistical method was used to predetermine sample size, and no data were excluded from the analyses. Experiments were conducted in triplicate. Statistical analysis was performed using GraphPad Prism 9 software with one-way ANOVA (three or more data groups were compared) to generate *P*-values. *P*-values ≤ 0.05 were considered significant: *$P < 0.05$, **$P < 0.01$, ***$P < 0.001$, and ****$P < 0.0001$. Data are presented as mean ± SD in all figures in which error bars are shown.

Reporting summary

Further information on research design is available in the Nature Portfolio Reporting Summary linked to this article.

Data availability

The next-generation sequencing data supporting the findings of P1 and P2 in this study have been uploaded to the European Genome-Phenome Archive (EGA) (Accession data - Study: EGAS50000000578, Dataset: EGAD50000000825 [https://ega-archive.org/datasets/EGAD50000000825]) and are available upon request from the corresponding authors (A.V.M., V.H., and H.L.S.). WGS and phenotypic data for the participants enrolled in the 100,000 Genomes Project (P3 and P5) are under restricted access. All data analyses for P3 and P5 were carried out within the secure Genomics England Research Environment, and no data can be copied or removed from the environment to ensure patient anonymity and data security under the approved ethics. Detailed phenotypic data were obtained directly from the referring clinicians who were contacted through the 100,000 genomic England research environment, and informed consent was obtained from human research participants and their guardians. The 100,000 Genomes Project NGS data are accessible by all researchers registered to join the Genomics England Research Network via the following link: https://www.genomicsengland.co.uk/research/academic. Access to the Research Environment can be granted following successful application review, which takes up to 10 working days, validation of applicants' affiliation to their institutes, and completion of the online information governance training. Source data are provided in this paper.

References

1. Murray, P. G., Clayton, P. E. & Chernausek, S. D. A genetic approach to evaluation of short stature of undetermined cause. *Lancet Diabetes Endocrinol.* **6**, 564–574 (2018).

2. Sovio, U. et al. Genetic determinants of height growth assessed longitudinally from infancy to adulthood in the Northern Finland Birth Cohort 1966. *PLoS Genet.* **5**, e1000409 (2009).

3. Storr, H. L. et al. Nonclassical GH insensitivity: Characterization of mild abnormalities of GH action. *Endocr. Rev.* **40**, 476–505 (2019).

4. Klammt, J. et al. Dominant-negative STAT5B mutations cause growth hormone insensitivity with short stature and mild immune dysregulation. *Nat. Commun.* **9**, 2105 (2018).

5. Vidarsdottir, S. et al. Clinical and biochemical characteristics of a male patient with a novel homozygous STAT5b mutation. *J. Clin. Endocrinol. Metab.* **91**, 3482–3485 (2006).

6. Bezrodnik, L. et al. Long-term follow-up of STAT5B deficiency in three Argentinian patients: Clinical and immunological Ffeatures. *J. Clin. Immunol.* **35**, 264–272 (2015).

7. Hwa, V. Human growth disorders associated with impaired GH action: Defects in STAT5B and JAK2. *Mol. Cell Endocrinol.* **519**, 111063 (2021).

8. Krone, K. A. et al. Signal transducer and activator of transcription 5B deficiency–associated lung disease. *Am. J. Respir. Crit. Care Med.* **205**, 1245–1250 (2022).

9. Smith, M. R., Satter, L. R. F. & Vargas-Hernández, A. STAT5b: A master regulator of key biological pathways. *Front Immunol.* **13**, 1025373 (2023).

10. Wittke, I. et al. Neuroblastoma-derived sulfhydryl oxidase, a new member of the sulfhydryl oxidase/quiescin6 family, regulates sensitization to interferon γ-induced cell death in human neuroblastoma cells. *Cancer Res.* **63**, 7742–7752 (2003).

11. Morel, C. et al. Involvement of sulfhydryl oxidase QSOX1 in the protection of cells against oxidative stress-induced apoptosis. *Exp. Cell Res.* **313**, 3971–3982 (2007).

12. Li, Y. et al. QSOX2 is an E2F1 target gene and a novel serum biomarker for monitoring tumor growth and predicting survival in advanced NSCLC. *Front. Cell Dev. Biol.* **9**, 688798 (2021).

13. Okada, Y. et al. A genome-wide association study in 19 633 Japanese subjects identified LHX3-QSOX2 and IGF1 as adult height loci. *Hum. Mol. Genet.* **19**, 2303–2312 (2010).

14. Yengo, L. et al. A saturated map of common genetic variants associated with human height. *Nature* **610**, 704–712 (2022).

15. Carlsson, L. M. S. Partial growth hormone insensitivity in childhood. *Baillière's Clin. Endocrinol. Metab.* **10**, 389–400 (1996).

16. Attie, K. M., Carlsson, L. M. S. & Rundle, A. C. Evidence for partial growth hormone (gh) insensitivity among "Idiopathic" short stature (iss) patients treated with growth hormone. *Pediatr. Res.* **33**, S48–S48 (1993).

17. Kofoed, E. M. et al. Growth hormone insensitivity associated with a STAT5b mutation. *N. Engl. J. Med.* **349**, 1139–1147 (2003).

18. Vairamani, K. et al. Novel dominant-negative GH receptor mutations expands the spectrum of GHI and IGF-I deficiency. *J. Endocr. Soc.* **1**, 345–358 (2017).

19. Steinhaus, R. et al. Mutationtaster2021. *Nucleic Acids Res.* **49**, W446–W451 (2021).

20. GTEx Consortium. The GTEx consortium atlas of genetic regulatory effects across human tissues. *Science* **369**, 1318–1330 (2020).

21. Ghoussaini, M. et al. Open targets genetics: systematic identification of trait-associated genes using large-scale genetics and functional genomics. *Nucleic Acids Res.* **49**, D1311–D1320 (2021).

22. Desmet, F.-O. et al. Human splicing finder: an online bioinformatics tool to predict splicing signals. *Nucleic Acids Res* **37**, e67 (2009).

23. Shamsani, J. et al. A plugin for the Ensembl Variant Effect Predictor that uses MaxEntScan to predict variant spliceogenicity. *Bioinformatics* **35**, 2315–2317 (2019).

24. Chueh, F.-Y., Leong, K.-F. & Yu, C.-L. Mitochondrial translocation of signal transducer and activator of transcription 5 (STAT5) in leukemic T cells and cytokine-stimulated cells. *Biochem. Biophys. Res. Commun.* **402**, 778–783 (2010).

25. Chueh, F.-Y., Chang, Y.-L., Wu, S.-Y. & Yu, C.-L. Signal transducer and activator of transcription 5a (STAT5a) represses mitochondrial gene expression through direct binding to mitochondrial DNA. *Biochem. Biophys. Res. Commun.* **527**, 974–978 (2020).

26. Tresse, E. et al. IFN-β rescues neurodegeneration by regulating mitochondrial fission via STAT5, PGAM5, and Drp1. *EMBO J.* **40**, e106868 (2021).

27. He, M. et al. Meta-analysis of genome-wide association studies of adult height in East Asians identifies 17 novel loci. *Hum. Mol. Genet.* **24**, 1791–1800 (2015).

28. Lango Allen, H. et al. Hundreds of variants clustered in genomic loci and biological pathways affect human height. *Nature* **467**, 832–838 (2010).

29. Han, S. et al. Identification of exon skipping events associated with Alzheimer's disease in the human hippocampus. *BMC Med. Genom.* **12**, 13 (2019).

30. Kingdom, R. & Wright, C. F. Incomplete penetrance and variable expressivity: From clinical studies to population cohorts. *Front. Genet.* **13**, 920390 (2022).

31. Russo, M. et al. Variable phenotypes are associated with PMP22 missense mutations. *Neuromuscul. Disord.* **21**, 106–114 (2011).

32. Shen, N. et al. Co-expression of phenylalanine hydroxylase variants and effects of interallelic complementation on in vitro enzyme activity and genotype-phenotype correlation. *Mol. Genet. Metab.* **117**, 328–335 (2016).

33. Saeed, S. et al. Loss-of-function mutations in ADCY3 cause monogenic severe obesity. *Nat. Genet.* **50**, 175–179 (2018).

34. Pugliese-Pires, P. N. et al. A novel STAT5B mutation causing GH insensitivity syndrome associated with hyperprolactinemia and immune dysfunction in two male siblings. *Eur. J. Endocrinol.* **163**, 349–355 (2010).

35. Vargas-Hernández, A. et al. Human STAT5b mutation causes dysregulated human natural killer cell maturation and impaired lytic function. *J. Allergy Clin. Immunol.* **145**, 345–357 (2020).

36. Cohen, A. C. et al. Cutting edge: Decreased accumulation and regulatory function of CD4+CD25high T cells in human STAT5b deficiency1. *J. Immunol.* **177**, 2770–2774 (2006).

37. Caldirola, M. S., Rodríguez Broggi, M. G., Gaillard, M. I., Bezrodnik, L. & Zwirner, N. W. Primary immunodeficiencies unravel the role of IL-2/CD25/STAT5b in human natural killer cell maturation. *Front. Immunol.* **9**, 1429 (2018).

38. Pelham, S. J. et al. STAT5B restrains human B-cell differentiation to maintain humoral immune homeostasis. *J. Allergy Clin. Immunol.* **150**, 931–946 (2022).

39. Walenkamp, M. J. E. et al. Growth hormone secretion and immunological function of a male patient with a homozygous STAT5b mutation. *Eur. J. Endocrinol.* **156**, 155–165 (2007).

40. Catli, G. et al. Atypical STAT5B deficiency, severe short stature and mild immunodeficiency associated with a novel homozygous STAT5B Variant. *Mol. Cell. Endocrinol.* **559**, 111799 (2023).

41. Paldino, G. et al. Analysis of a series of Italian APECED patients with autoimmune hepatitis and gastro-enteropathies. *Front. Immunol.* **14**, 1172369 (2023).

42. Tanno, A. et al. Decreased expression of a phagocytic receptor Siglec-1 on alveolar macrophages in chronic obstructive pulmonary disease. *Respir. Res.* **21**, 30 (2020).

43. Villamayor, L. et al. The IFN-stimulated gene IFI27 counteracts innate immune responses after viral infections by interfering with RIG-I signaling. *Front. Microbiol.* **14**, 1176177 (2023).

44. Lee, J. E. et al. Nongenomic STAT5-dependent effects on Golgi apparatus and endoplasmic reticulum structure and function. *Am. J. Physiol.-Cell Physiol.* **302**, C804–C820 (2012).

45. Zhang, L. et al. Mitochondrial STAT5A promotes metabolic remodeling and the Warburg effect by inactivating the pyruvate dehydrogenase complex. *Cell Death Dis.* **12**, 1–12 (2021).

46. Finsterer, J. & Frank, M. Gastrointestinal manifestations of mitochondrial disorders: a systematic review. *Ther. Adv. Gastroenterol.* **10**, 142–154 (2017).

47. Dubé, P. E., Forse, C. L., Bahrami, J. & Brubaker, P. L. The essential role of insulin-like growth factor-1 in the intestinal tropic effects of glucagon-like peptide-2 in mice. *Gastroenterology* **131**, 589–605 (2006).

48. Chernausek, S. D. et al. Long-term treatment with recombinant insulin-like growth factor (IGF)-I in children with severe IGF-I deficiency due to growth hormone insensitivity. *J. Clin. Endocrinol. Metab.* **92**, 902–910 (2007).

49. Jumper, J. et al. Highly accurate protein structure prediction with AlphaFold. *Nature* **596**, 583–589 (2021).

50. Rodrigues, C. H., Pires, D. E. & Ascher, D. B. DynaMut: predicting the impact of mutations on protein conformation, flexibility and stability. *Nucleic Acids Res.* **46**, W350–W355 (2018).

51. Capriotti, E., Fariselli, P. & Casadio, R. I-Mutant2.0: predicting stability changes upon mutation from the protein sequence or structure. *Nucleic Acids Res.* **33**, W306–W310 (2005).

52. Worth, C. L., Preissner, R. & Blundell, T. L. SDM—a server for predicting effects of mutations on protein stability and malfunction. *Nucleic Acids Res.* **39**, W215–W222 (2011).

53. Pires, D. E. V., Ascher, D. B. & Blundell, T. L. DUET: a server for predicting effects of mutations on protein stability using an integrated computational approach. *Nucleic Acids Res.* **42**, W314–W319 (2014).

54. Cheng, J., Randall, A. & Baldi, P. Prediction of protein stability changes for single-site mutations using support vector machines. *Proteins Struct. Funct. Bioinform.* **62**, 1125–1132 (2006).

55. Pires, D. E. V., Ascher, D. B. & Blundell, T. L. mCSM: predicting the effects of mutations in proteins using graph-based signatures. *Bioinformatics* **30**, 335–342 (2014).

56. McGuffin, L. J. et al. Prediction of protein structures, functions and interactions using the IntFOLD7, MultiFOLD and ModFOLDdock servers. *Nucleic Acids Res.* **51**, W274–W280 (2023).

57. Tomkins, J. E. et al. PINOT: an intuitive resource for integrating protein-protein interactions. *Cell Commun. Signal.* **18**, 92 (2020).

58. Jones, D. T. & Cozzetto, D. DISOPRED3: precise disordered region predictions with annotated protein-binding activity. *Bioinformatics* **31**, 857–863 (2015).

59. Nugent, T. & Jones, D. T. Transmembrane protein topology prediction using support vector machines. *BMC Bioinform.* **10**, 159 (2009).

60. Gardner, E. J. et al. Damaging missense variants in IGF1R implicate a role for IGF-1 resistance in the etiology of type 2 diabetes. *Cell Genom.* **2**, None (2022).

61. McLaren, W. et al. The ensembl variant effect predictor. *Genome Biol.* **17**, 122 (2016).

62. Loh, P.-R. et al. Efficient Bayesian mixed-model analysis increases association power in large cohorts. *Nat. Genet.* **47**, 284–290 (2015).

63. Saari, A. et al. New Finnish growth references for children and adolescents aged 0 to 20 years: Length/height-for-age, weight-for-length/height, and body mass index-for-age. *Ann. Med.* **43**, 235–248 (2011).

64. Maharaj, A. et al. Predicted benign and synonymous variants in CYP11A1 cause primary adrenal insufficiency through missplicing. *J. Endocr. Soc.* **3**, 201–221 (2019).

65. Guesdon, F. et al. Expression of a glycosylphosphatidylinositol-anchored ligand, growth hormone, blocks receptor signalling. *Biosci. Rep.* **32**, 653–660 (2012).

66. Ran, F. A. et al. Genome engineering using the CRISPR-Cas9 system. *Nat. Protoc.* **8**, 2281–2308 (2013).

67. Kelly, A., Tang, R., Becker, S. & Stanley, C. A. Poor specificity of low growth hormone and cortisol levels during fasting hypoglycemia for the diagnoses of growth hormone deficiency and adrenal insufficiency. *Pediatrics* **122**, e522–e528 (2008).

68. Chesover, A. D. & Dattani, M. T. Evaluation of growth hormone stimulation testing in children. *Clin. Endocrinol.* **84**, 708–714 (2016).

Author contributions

A.V.M. conceptualised the project, performed the experimental work, and conducted data acquisition and analysis. M.I. conducted data mining of the 100KG database, and A.V.M. and M.I. analysed genomic sequencing data. A.J. and K.K. conducted FINRISK population data mining and genetic association analysis. L.J.M. performed in silico protein predictions and modelling. R.Y.J. and J.R.B.P. conducted exome-wide burden testing of UK Biobank study data. A.V.M., A.R., R.E., E.O.T., F.E., A.J., H.L.S., and A.A. collected clinical data and provided patient material. All authors contributed to the writing of the manuscript. A.V.M., V.H., and H.L.S. coordinated the project and wrote the report.

Competing interests

The authors declare no competing interests.

Additional information